

**Development of cell-based assay to investigate relationships between cell cycle and
programmed cell death**

(細胞周期及びプログラム細胞死の関係性の検討のための細胞基盤試験法の開発)

A Thesis

By

MD. SHAZADUR RAHMAN

Student ID: 20DS056

DOCTOR OF PHILOSOPHY (PhD)

IN

SCIENCE AND ENGINEERING

September 2024



Graduate school of Science and Engineering, Saitama University

Saitama 338-8570, Japan

**Development of cell-based assay to investigate relationships between cell cycle and
programmed cell death**

(細胞周期及びプログラム細胞死の関係性の検討のための細胞基盤試験法の開発)

A Thesis

By

MD. SHAZADUR RAHMAN

Student ID: 20DS056

A Dissertation Submitted to

The Graduate school of Science and Engineering, Saitama University, Japan

In partial fulfillment of the requirements for the degree of

DOCTOR OF PHILOSOPHY (PhD)

IN

SCIENCE AND ENGINEERING

September 2024



Graduate school of Science and Engineering, Saitama University

Saitama 338-8570, Japan



**Development of cell-based assay to investigate relationships between cell cycle and
programmed cell death**
(細胞周期及びプログラム細胞死の関係性の検討のための細胞基盤試験法の開発)


By
MD. SHAZADUR RAHMAN
Student ID: 20DS056

**A Dissertation Submitted to
The Graduate school of Science and Engineering, Saitama University, Japan
In partial fulfillment of the requirements for the degree of**


**DOCTOR OF PHILOSOPHY (PhD)
IN
SCIENCE AND ENGINEERING**

September 2024


Approved By:



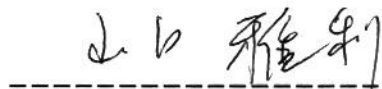
Professor Dr. Miho Suzuki
Supervisor and
Chairman, Examination Committee



Professor Dr. Naoto Nemoto
Co-supervisor and
Member, Examination Committee



Professor Dr. Koji Matsuoka
Co-supervisor and
Member, Examination Committee



Professor Dr. Masatoshi Yamaguchi
Co-supervisor and
Member, Examination Committee

Acknowledgments

All glory belongs to Almighty Allah, who has shown me mercy and faith in my capability to complete the research work. I would like to express my heartfelt gratitude to Professor Dr. Miho Suzuki, my advisor, for her constant supervision, encouragement, and valuable suggestions during my PhD study. Without her persistent help, this thesis would not have been possible. I also thank her for teaching me how to be a professional researcher, effective writing and presentation skills for career development. I would like to express my sincere appreciation and indebtedness to Professor Dr. Naoto Nemoto, Professor Dr. Koji Matsuoka and Professor Dr. Masatoshi Yamaguchi for the constructive feedback and advise for strengthened my knowledge and encouraged me for the research work.

I convey my gratitude to the Ministry of Education, Culture, Sports, Science, and Technology (MEXT) Japan for a Grant-in-Aid for Scientific Research. I would like to thank Professor Dr. Ichiro Sakata for giving me the opportunity of flow cytometry studies in his lab. Sincere gratitude is also to all the lab members for their wonderful collaboration and actuation during the course of the study.

Lastly, my deep and boundless gratitude to my family members for their love, support, encouragement and sacrificed their happiness along with this journey. Finally, thanks to my friends and all well-wishers for their assist and friendly cooperation during my study.

Abstract

Live cell imaging or high-content imaging system have enthusiastically been developed for comprehensive understanding of cellular phenomena. Especially huge number of molecular sensors have been exploited to monitor various target phenomena. In some cases, more than two distinguish events were observed at a time in a single cell. However, it might still be challenge in cases of living cell population analysis simultaneously for some signaling steps, namely, high-content imaging due to elaborate sensing mechanisms. In this study, our aim is to obtain inclusive knowledges about various programmed cell deaths caused upon apoptosis induction chemicals with cell cycle phases. To accomplish our aim, by live cell statistical imaging analysis with normalized and expandable molecular sensors, we have prepared FRET based molecular sensors combination of fluorescent proteins (FP) and fluorescent dyes for detection in vitro, cell division with cell cycle phases, programmed cell deaths simultaneously. We have selected separase and caspases as index for cell division and programmed cell death respectively. And finally, we investigate the relationship between cell cycle and programmed cell deaths of cell population analysis by detecting protease activity and live monitoring in living cells.

Table of Contents

Title	Page No.
Acknowledgements	iv
Abstract	v
List of tables	vii
List of figures	vii-ix
List of abbreviations	x
Chapter 1 Background	
General introduction	1-2
Chapter 2 Live cell monitoring of separase activity upon cell cycle progression	
2.1 Abstract	3
2.2 Introduction	3-6
2.3 Materials and methods	6-11
2.4 Results and discussion	11-20
2.5 Conclusion	20-21
Chapter 3 Live cell monitoring of separase commitment to apoptosis	
3.1 Abstract	21
3.2 Introduction	21-24
3.3 Materials and methods	24-26
3.4 Results and discussion	26-31
3.5 Conclusion	31-32
References	32-40
Appendix	41-42

List of Tables

- Table 1: Emission ratios of FRET-based GFP and RFP molecular sensors for separase and caspase-3 sensing
- Table 2: Some molecular sensors estimated Förster radius value

List of figures

- Figure 1: Sensing mechanism of FRET based separase sensors
- Figure 2: Emission patterns of molecular sensors excited at 488 nm. Pattern associations were shown in the inset
- Figure 3: Flow cytometric confirmation of molecular sensors for separase-sensing uptake into HeLa cells by dot plot analysis
- Figure 4: Fluorescence microscopic observation to compare two types of molecular sensor localizations in cells. It appeared that not localized type of molecular sensor (WNLS based) stays at endosome surrounding the nucleus to disperse into the cytosol. On the other hand, nucleus localized type of molecular sensor (NLS based) appeared to be accumulated inside nucleus.
- Figure 5: DNA amount in FBS-supplied (100% FBS) and FBS-starved (0% FBS) HeLa cells stained with ethidium bromide (A, B) and propidium iodide (C, D).
- Figure 6: Separase expression profiles of cell cycle synchronized 0 h and 24 h. Blue arrow heads point to assigned bands as intact and autocleavage of separase. Comparable patterns were obtained from two more lysate preparations
- Figure 7: Separase activity validation contained in lysate preparations. (A) Emission pattern changes of molecular sensors through lysate treatments. (B) Increasing

ratio of FRET efficiencies through lysate treatments

Figure 8: Separase activity monitoring through cell cycle progression. (A) Fluorescence microscopic observation of molecular sensor localization inside cells. (B) The emission profiles in HeLa cells after 0 h and 24 h incubation in culture medium containing serum. Fluorescence intensity was normalized at isosbestic point. (C) FRET efficiency exchanges before and after cell cycle progression (Before: $n = 55$ cells from three different experiments, After: 34 cells from three different experiments). Error bars: S.E.M. *: $p < 0.05$ in Student's t-test

Figure 9: Separase activity monitoring through cell cycle progression. (A) Cell cycle control experimental flow was schematically drawn. (B) FRET efficiencies (after 0 h and 24 h incubation) were approximately estimated using median values from histograms for FRET efficiencies. (C) Increasing ratios for FRET efficiencies of 0 h and 24 h were calculated for NLS- and WNLS-based molecular-sensor-introduced cell populations

Figure 10: Changes in the emission patterns of molecular sensors on in vitro treatment with caspase-3 for GFP-based separase (A) and caspase-3 (B) sensing sensors (Caspase-3 presence (orange) and absence (blue)).

Figure 11: Uptake efficiency of chimeric FRET-Based caspase-3 sensing RFP sensor into cell-cycle-controlled HeLa cells (A) and FRET efficiencies were estimated using histograms with anti-cancer drug treatments by flow cytometry (B).

Figure 12: Uptake efficiency of chimeric FRET-Based GFP and RFP based bioprobes for separase and caspase-3 sensing into cell-cycle-controlled HeLa cells. (A and C) and Flow Cytometry FRET efficiencies were estimated using histograms with

anti-cancer drug treatments (B and D).

Figure 13: Microscopic observation of HeLa cells in the presence and absence of molecular sensors with anticancer drug treatments.

Figure 14: Identification of different cell states upon NLS based molecular sensor uptake using fluorescence microscopic observations in detail. Although forms of introduced cells were varied as a spherical shape or spread one, they still exhibited identical localization patterns for molecular sensors.

List of abbreviations

FRET- Fluorescence Resonance Energy Transfer

FP- Fluorescent Proteins NLS- Nuclear

Localization Signal

GFP- Green Fluorescent Protein

Plk1- Polo like kinase1

LB- Luria Bertani

BPER- Bacterial Protein Extraction Reagent

Ni²⁺-NTA - Nitrilotriacetic acid

IPTG- Isopropyl- β -D-thiogalactopyranoside

PBS- Phosphate Buffered Saline

DTT- Dithiothreitol

DMEM- Dulbecco's Modified Eagle Medium

EDTA- Ethylenediamine Tetraacetic Acid

FACS- Fluorescence Activated Cell Sorter

PIPES- 2-[4-(2-sulfoethyl) piperazin-1-ium-1-yl] ethanesulfonate

CHAPS- 3- [dimethyl(3- {[(3 α ,5 β ,7 α ,12 α)-3,7,12-trihydroxy-24-oxocholan-24yl] amino } propyl) ammonio] propane-1-sulfonate

TNF- Tumor Necrosis Factor

CHX- Cycloheximide

DOC-Docetaxel

NaCl- Sodium chloride

Chapter I: General Introduction

Multicellular organisms are functioned with many biological activities to maintain individuals over cell continuations. Cell cycle and programmed cell deaths are two representative activities for the individual maintenances. The programmed cell deaths are classified into numerous categories based on involved molecules [Elmore et al. 2007; Galluzzi et al. 2018; Tang et al. 2019; Nirmala and Lopus 2020]. Various caspases (cysteine aspartate-specific protease) engaging the cell deaths have been found as key molecules for the pathways and utilized for the classification. However, we could not unravel that what kind of triggers and processes could cause and complete different cell deaths in detail yet. On the other hand, many cellular phenomena are strictly regulated not only by single cell level but also by cell population level. We have focused on a cell cycle for cell divisions as the opposite cellular phenomena of the cell deaths. Examining the dynamics of the cell cycle in conjunction with cell deaths in cultured cancer cell lines can help researchers better understand how cell deaths are regulated for multicellular organisms.

The cell cycle is dynamic cellular processes that cause cell divide into two daughter cells and consist of two main stages as interphase and mitotic phase. The separation of sister chromatids is an irreversible process that occurs in mitotic phase and is one of the most dramatic cellular processes during cell cycle. The two key events underlying this step are the removal of cohesin, protein complex for sister chromatids interactions between sister chromatids and the subsequent poleward movement of disjoined sisters [Oliveira and Nasmyth 2010]. The former event is mediated by proteolysis with separase, which cleaves the cohesion complex that physically holds sister chromatids together. In most eukaryotes, the activity of separase is controlled by its inhibitory chaperone securin through phosphorylation and ubiquitination. The latter event involves proteins that regulate microtubule constructions, including microtubule depolymerization with α and β tubulins and biomolecule transports for the both end of microtubule with kinesin super family [Rogers et al. 2004; Wolf et al. 2006]. There are still unknown mechanisms comprehensively that coordinate these proteins, but somewhat depend on decreases in cdk1 activity and increases in ubiquitin ligase which need to induce microtubule

dynamics to pull disjoined sister chromatids apart [Oliveira et al. 2010]. These indispensable events must be connected, organized and occurred concurrently on all chromosomes.

Cell death is a cellular phenomenon that lose its function resulting of natural process for replacement by new one or causing by external factors such as diseases, infections and injuries. The former cell death is programmed cell death, apoptosis and autophagy are categorized into this type of cell death as typical ones. There are so many types of programmed cell deaths identified and classified using proteins involved respective types. On the contrary, necrosis is the latter cell death as non-physiological phenomena. Caspases (cysteine aspartate-specific protease) is a member of the family of endoproteases playing essential roles in programmed cell death, mainly degrading some compounds inside cells for achievement of the cell death along with minimum effects on the neighboring cells. Caspases have a role in inflammation by processing pro-inflammatory cytokines to recruit immune cells as well. There are other characterized roles of caspases. Most caspases are identified as functions in programmed cell deaths as initiation, execution and others. [McIlwain et al. 2013]. Caspase-3 is known as an executioner caspase in apoptosis because of its role in coordinating the destruction of cellular important components such as DNA fragmentation or degradation of cytoskeletal proteins. The activity of caspase-3 is tightly regulated, and it is produced as precursor in an inactive pro-form [Zhang et al. 2013] and activated with other caspase of upstream in apoptotic signaling flow. Owing to this key role, caspase-3 is exploited intracellularly as a target of control of apoptosis for therapeutic outcomes.

Live cell imaging can be useful techniques to investigate molecular processes related to various cellular phenomena. Many molecular sensors have been generated to track various target phenomena of signaling pathways [Diana Pendin et al. 2017] by live cell imaging. As a result, monitoring as many of the key cellular processes as feasible in a single cell would be beneficial [Schultz et al. 2005]. Due to complicated cross-talk of signaling pathways and response heterogeneities, there are still some obstacles. In this investigation, we have introduced normalized FRET-based molecular sensors for separase and caspase-3 to monitor both reactions simultaneously in a cell population analysis that could correlate cell cycle with apoptotic cell death.

Chapter II: Live Cell Monitoring of Separase Activity with Chimeric FRET-Based Molecular Sensors upon Cell Cycle Progression

2.1 Abstract

Separase is a key cysteine protease in the separation of sister chromatids through the digestion of the cohesin ring that inhibits chromosome segregation as a trigger of the metaphase–anaphase transition in eukaryotes. Its activity is highly regulated by binding with securin and cyclinB-CDK1 complex. These bindings prevent the proteolytic activity of separase until the onset of anaphase. Chromosome missegregation and aneuploidy are frequently observed in malignancies. However, there are some difficulties in biochemical examinations due to the instability of separase *in vitro* and the fact that few spatiotemporal resolution approaches exist for monitoring live separase activity throughout mitotic processes. Here, we have developed FRET-based molecular sensors, including GFP variants, with separase-cleavable sequences as donors and covalently attached fluorescent dyes as acceptor molecules. These are applicable to conventional live cell imaging and flow cytometric analysis because of efficient live cell uptake. We investigated the performance of equivalent molecular sensors, either localized or not localized inside the nucleus under cell cycle control, using flow cytometry. Synchronized cell cycle progression rendered significant separase activity detections in both molecular sensors. We obtained consistent outcomes with localized molecular sensor introduction and cell cycle control by fluorescent microscopic observations. We thus established live cell separase activity monitoring systems that can be used specifically or statistically, which could lead to the elucidation of separase properties in detail.

2.2 Introduction

Separase is a large eukaryotic endopeptidase (140-250 kD) belonging to the cysteine protease family [Uhlmann et al. 2000] which performs critical functions in the maintenance of genetic homeostasis. Cells need to maintain genome stability during cell division to preserve and transmit their hereditary material intact to the next generation [Jackson et al. 2009]. The cell cycle is a dynamic biological process that causes cells to divide into two daughter cells, and the most dramatic cellular phenomenon involved in the cell cycle is the irreversible separation of sister chromatids, which happens during the mitotic phase, specifically at the metaphase–

anaphase transition in eukaryotes. These precisely controlled processes are triggered by separase activation which is tightly regulated by its inhibitory chaperone, securin [Ciosk et al. 1998; Uhlmann et al. 1999; Henschke et al. 2019]. Securin stabilizes separase by co-translational binding to assist its correct folding [Jallepalli and Lengauer 2001]. The CDK-1 in vertebrates phosphorylates to connect phosphorylated separase and cyclin B1 to form the other controlling complex for separase activity [Gorr et al. 2005; Sanchez-Puig et al. 2005; Csizmok et al. 2008].

Generally, separase has vital roles in many cellular functions, besides chromosome segregation during mitosis and meiosis [Uhlmann et al. 2000; Ciosk et al. 1998; Buonomo et al. 2000], DNA damage repair [Nagao et al. 2004; McAleenan et al. 2013; Hellmuth et al. 2018], centrosome disengagement and duplication [Tsou et al. 2009; Lee et al. 2012], and spindle stabilization and elongation [Papi et al. 2005; Baskerville et al. 2008]. The proteins astrin and Aki1 function as inhibitors of centrosomal separase [Thein et al. 2007] and these combinations engage in proper spindle function in mitosis [Nakamura et al. 2009]. Separase disintegrates the cohesion between sister chromatids by cleaving one of the subunits Scc1/Rad21/Mcd1 from the cohesin ring for chromosomal segregation [Hauf et al. 2001]. Cohesin is the “glue” that binds the mother and daughter centrioles, and cleavage of this pool of cohesin by separase encourages centriole disengagement, according to various biochemical investigations [Schockel et al. 2011]. Interestingly, separase cleaves both the cohesin subunits Scc1/Rad21/Mcd1 and kendrin/pericentrin B at the centrosome [Matsuo et al. 2012]. But separase is well known to indicate the minimal consensus motif as ExxR at cleavage sites [1,4,22]. Separase activation is elicited by destruction of securin [Funabiki et al. 1996; Cohen-Fix et al. 1996; Rao et al. 2001] and cyclin B1 [Gorr et al. 2005] by the proteasome degradation system after ubiquitination with anaphase-promoting complex/cyclosome (APC/C) [Zachariae et al. 1996; Peters 2002, Zou et al. 2002]. Additional mechanisms for the separase activation process have been reported, such as that auto-cleavage of separase is needed to promote mitosis, but not to enhance protease activity [Papi et al. 2005; Zou et al. 2002; Herzig et al. 2002; Chestukhin et al. 2003]. These activation profiles are directed through phosphorylation states of separase including specific protein phosphatase 2A [Holland et al. 2007; Hellmuth et al. 2014; Agarwal et al. 2002]. The molecular mechanisms underlying separase behaviors have been revealed by recent structural studies [Lin et al. 2016; Luo and Tong 2017; Boland et al. 2017].

However, there are still questions remaining about the activities and regulation of separase activities which can be clarified with biochemical approaches. It is partially due to problems in defective expression systems that it is difficult to obtain active separase unassisted by a chaperone protein [Hornig et al. 2002; Hellmuth et al. 2014]. It is possible for anti-cancer medications to establish an index that will normalize excessive or insufficient separase activities. Therefore, in this investigation, we try to detect separase activity in mammalian live cells through FRET-based sensing by changing intramolecular FRET efficiencies upon enzymatic reactions. We have designed a chimeric FRET-based molecular sensor that utilizes a green fluorescent protein (GFP) mutant (donor molecule) with separase-cleavable sequences followed by unique cysteine for chemical modification with a fluorescent organic dye (acceptor molecule) as a simple conjugate (Figure 1) [Zhang et al. 2005]. We could easily replace the donor fluorescent protein, recognition sequences, and dye species to optimize the assay system [Suzuki et al. 2022]. Furthermore, the molecular sensor can efficiently be delivered into live cells via endocytotic pathways. Here, we have attempted to localize our molecular sensor for monitoring organelle-specific events such as separase activations. We introduced microscopic observation to confirm our aim, and flow cytometric analysis to check the variety in the activation extent for separase during cell cycle progression, using a molecular sensor localized inside the nucleus as well as a non-localized one. We succeeded in detecting separase activations upon pushing the cell cycle forward in every case equally, demonstrating that our robust molecular sensor functioned beyond existing approaches. The achievable flow cytometric separase assay would render the range of intracellular variation in separase activity or its alteration upon anti-cancer drug treatment in combination with other fluorescent markers or microscopically detailed observations. Very impressively, the versatile molecular sensor contributory systems we developed here can potentially not only monitor the dynamics of separase in situ, but also can assess the real-time therapeutic efficacy of cancer treatment.

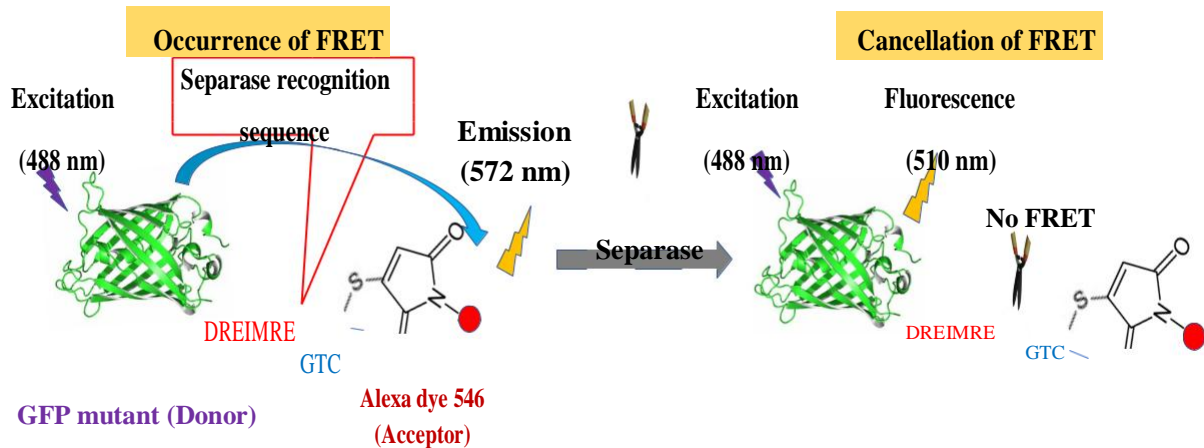


Figure 1: Sensing mechanism of FRET based separase sensors

2.3 Materials and methods

2.3.1 Plasmid Construction for Separase Activity Detection with or without Nuclear Localization Sequence (NLS)

Inverse polymerase chain reaction (iPCR) [Imai et al. 1991] was used to construct a plasmid containing the reporter genes for GFP and to detect separase activity. This plasmid was based on the pUV5casS52tag for caspase-3 activity sensing [Alnemri et al. 1996; Suzuki et al. 2012] and the first manipulation was carried out to replace DEVD-coded regions with DREIMRE around the C-terminal and to adjust linker sequences for the accessibility of the target enzyme referring to the molecular sensor for caspase-9 because of its structural similarity with separase, to create pUV5Sep. The second manipulation included the insertion of GPKKKRKV (NLS) [Kalderon et al. 1984; Kitamura et al. 2015] around the N-terminal to obtain pUV5SepNLS. The genetic manipulations above were certified by the usual method for gene sequencing. Coded amino acid sequences for the three GFP variants mentioned above are shown in Appendix 1.

2.3.2 Chimeric FRET-Based Molecular Sensor Preparation

Two variant green fluorescent proteins (GFP) were isolated initially. The two plasmids described above (pUV5Sep and pUV5SepNLS) were transfected into *Escherichia coli* BL21 cells (DE3). The transfected bacteria were cultured in Luria Bertani (LB) medium containing 75 $\mu\text{g/mL}$ of ampicillin; the expression of the GFP derivatives was induced by isopropyl- β -D-

thiogalactopyranoside (IPTG). The bacteria were harvested and lysed with a sufficient amount of bacterial protein extraction reagent, B-PER II (Thermo Scientific Pierce, Rockford, IL, USA). Each target protein was isolated from the lysate by centrifugation for separation from cell debris and purified using Ni²⁺-NTA (nitrilotriacetic acid) affinity chromatography through (Histidine)₆ tag sequence fused with the GFP derivative. The remaining reagents were removed with a gel filtration column and recovered proteins were then reconstituted in phosphate-buffered saline (PBS) separately. Isolated fluorescent proteins (FP) were chemically modified with fluorescent dyes, namely Alexa Fluor-546 (Life Technologies, Carlsbad, CA, USA) (Thermo Scientific Pierce). Then, 10 μM of GFP dissolved in PBS was reduced with 1mM of dithiothreitol (DTT). Excess DTT was removed by gel filtration equilibrated with phosphate-buffered saline (PBS) (NICK column, GE Healthcare, Buckinghamshire, UK), and an aliquot of the eluate was immediately incubated with the corresponding fluorescent dye at the molar ratio of 1:10 at 37 °C for 4 h which was then allowed to stand at 4 °C for 6 h. Ultrafiltration (EMD, Millipore, Billerica, MA, USA) was used to remove unreacted dye and concentrate the solution to an adequate volume for use in future studies. The FRET efficiencies were assessed to check emission profiles excited at 488 nm by fluorescence spectroscopy using a Shimadzu RF-5300PC spectrophotometer (Shimadzu, Kyoto, Japan).

2.3.3 Evaluations for Separase Activity with Chimeric FRET-Based Molecular Sensor

We have already demonstrated that a requisite minimum formula to approximate FRET efficiency, fluorescence intensity of emission maxima for the donor molecule, and fluorescence intensity of emission maxima for the acceptor molecule could be applied to quantify target enzyme activities for most constructs of GFP variants and Alexa Fluor-532, 546, 555, 594, due to the high FRET efficiencies of the chimeric molecular sensors followed by calculations for increasing the ratio of FRET efficiencies [Suzuki et al. 2012]. GFP variants for caspase-3 and caspase-9 detections attached with Alexa Fluoro-546 were subjected to further evaluations as molecular sensors on the points by measuring fluorescence lifetime changes of donor molecules upon enzymatic reactions [Suzuki et al. 2015]. As estimated, the Förster radius for those constructs supported the high FRET efficiencies. Some extracted estimations are shown in Appendix 2.

2.3.4 Introduction of Chimeric FRET-Based Molecular Sensor into Cell-Cycle-Controlled HeLa Cells

The chimeric FRET-based molecular sensor was confirmed to be introduced into cells through straightforward methods by the incubation of cells with culture media including molecular sensors. We have already demonstrated efficient uptakes of many combinations of GFP variants and Alexa dyes into several cell types [Suzuki et al. 2012]. As endocytic pathways could be involved as mechanisms for the uptake due to partial inhibitions with some endocytic inhibitors and no effects at all from serum abundance or deprivation [unpublished data], we have thus introduced the chimeric FRET-based molecular sensor according to an approach based on cell cycle control. Subcultured HeLa cells were seeded into a culture dish filled with Dulbecco's Modified Eagle Medium (DMEM) supplied with 10% fetal bovine serum (FBS) at 37 °C under an atmosphere containing 5% CO₂. After confirmations of proper growth, the culture medium was replaced with DMEM without FBS to suppress cell cycle progression and incubated for 24 h at 37 °C under an atmosphere containing 5% CO₂. Following this, the culture medium was replaced with DMEM without FBS containing 5 μM of corresponding FRET-based molecular sensor for 12 h incubation at 37 °C under an atmosphere containing 5% CO₂. The residual FRET-based molecular sensor was removed by washing the cells with culture medium without FBS and subjected to further experiments.

2.3.5 Flow Cytometry

The HeLa cells introduced by the FRET-based molecular sensor, along with further experimentally processed cells, were rinsed with 250 μL of 0.2 mM EDTA. The chelating solution was removed to stock and the remaining cells were treated with 250 μL of Accutase and Accumax cell detachment solutions (Innovative Cell technologies, San Diego, CA, USA) for 5 min at 37 °C. The detached cell mixtures were recovered and combined with the stocked solutions. The remaining cells were completely detached with 250 μL of 0.25% trypsin solution. The resulting cell mixtures were added to all the combined solutions that had been so far produced at this point in the process. The culture plate was washed with 250 μL of PBS to be transferred to all the recovered solutions described above. The resulting solutions were filtered before being subjected to flow cytometry analysis using a SONY FACS machine (LE-SH800 SONY Co., Ltd. Tokyo Japan). The fluorescence intensity and other optical data of the harvested cell population (30,000 cells) were monitored by excitation using a 488-nm semiconductor laser

and adequate filter sets were selected to split donor (GFP variants) and acceptor (Alexa Fluor-546) emissions. FlowJo software (Becton, Dickinson and Company, San Jose, CA, USA) was used to process the collected data.

2.3.6 Image Acquisitions for FRET-Based Molecular Sensor Localizations in HeLa Cells

Approximate examination of molecular sensor localization was carried out at room temperature using an ECLIPSE TE 2000U (Nikon Solutions Co., Ltd., Tokyo, Japan) with a $\times 40$ water immersion objective lens. The FRET-based molecular sensor was excited with an ultra-high pressure mercury lamp through an adequate combination of a dichroic mirror and filter to detect GFP and Alexa 546 emissions and show bright images of each. The acquired images were processed with ImageJ supported by NIH.

2.3.7 Verification of Cell Cycle Control by Serum Starvation through DNA Amount Estimation

Harvested subconfluent cells were centrifuged at 15,000 rpm and resuspended in 1 mL of DMEM supplied with 10% FBS and 10% DMSO. The suspension was frozen for one hour at $-20\text{ }^{\circ}\text{C}$. The resulting materials were thawed and centrifuged at 15,000 rpm at $4\text{ }^{\circ}\text{C}$ to remove supernatant. Collected cells were resuspended to adjust recommended cell density as 1×10^6 cells per milliliter in 1 ml of ice-cold Hoechst staining buffer and incubated at $4\text{ }^{\circ}\text{C}$ for 15 min in the dark. Ethidium bromide was added to 1 g/mL solution and allowed to stand for 15 min at $4\text{ }^{\circ}\text{C}$ in the dark. All the solutions were filtrated and the DNA contents of the recovered cell solutions were determined using flow cytometric analysis as described above. Data analysis was performed with Flow Jo software correspondingly.

2.3.8 Western Blotting analysis for separase expression

Expression profiles of separase for cell populations in cell cycle arrest or its continuation were examined by Western blotting. HeLa cells cultured with DMEM supplied with or without 10% FBS for 24 h were collected individually by centrifugation at 15,000 rpm following trypsinization. The recovered cells were rinsed with aliquots of PBS by centrifugation by the

same method and lysed using M-PER™, Mammalian Protein Extraction Reagent (Thermo Fisher Scientific Inc., Waltham, MA, USA), according to the standard procedures as instructed by the supplier. Protein concentrations for recovered extracts were determined by spectrophotometer at 280 nm wavelength absorption. Denatured samples were applied to SDS PAGE and transferred to the PVDF membrane to carry out Western blotting using anti-Separase rabbit polyclonal antibody (abcam plc. Cambridge, UK) as the primary antibody, followed by detection of the 233 kDa full-length separase with Goat Anti-Rabbit IgG HL (Alexa Fluor-680) as the secondary antibody. Band assignment for the full-length and cleaved separase was carried out using prestained protein standard (Bio-Rad laboratories, Inc. Tokyo Japan). Protein extraction of cell lysates was verified for adjustment by glyceraldehyde 3-phosphate dehydrogenase (GAPDH) detection with GAPDH rabbit polyclonal antibody (Proteintech Group Inc. Tokyo, Japan). Band images were taken by fluorescent imager (Typhoon FLA 9500, GE Healthcare Japan, Tokyo, Japan).

2.3.9 Separase Activity Estimation Included in Cell-Cycle-Progressed Cell Lysate Preparation with FRET-Based Molecular Sensors

We examined the separase activity derived from the cell-cycle-progressed cell lysate preparations mentioned in Section 2.3.8 using two types of chimeric FRET-based molecular sensors which were NLS-based and WNLS-based. We developed a modified method that we utilized to validate the FRET-based molecular sensors in vitro with a commercially available enzyme. Briefly, 2 μ M of each FRET-based molecular sensor was incubated with the obtained cell lysate for 1 h. As a control experiment, we incubated the molecular sensors with aliquots of M-PER™. After 1 h of incubation, we assessed the emission profiles excited at 488 nm by fluorescence spectroscopy.

2.3.10 Separase Activations through Cell Cycle Progression

The HeLa cells introduced by the FRET-based molecular sensor, as described in Section 2.3.4, were divided into two populations. One population was harvested to be applied to flow cytometric analysis directly. The other populations were continuously exposed to DMEM

supplied with 10% FBS at 37 °C under an atmosphere containing 5% CO₂ for 24 h. Processed cells were then collected and analyzed by flow cytometry, as mentioned above.

2.3.11 Fluorescence Microscope Observation of Bioprobe Localization Inside Cells

The HeLa cells introduced by the FRET-based molecular sensor, described in Section 2.3.4, were divided into two populations. One population was observed immediately before the cell cycle restarted and the other was observed after 24 h of exposure to DMEM supplied with 10% FBS, as the population after cell cycle progression. Fluorescence imaging was performed at room temperature using an FV-1000 confocal microscope (Olympus, Tokyo, Japan) with a ×60 oil immersion objective lens. The FRET-based molecular sensor was excited at 488 nm from an Ar laser through a dichroic mirror (DM405/488/559). Fluorescence was separated at 560 nm by a dichroic mirror and detected by two photomultipliers through suitable band path filters: 500–545 nm for GFP and 570–670 nm for Alexa 546.

2.3.12 Imaging Analysis for molecular sensor localization and separate activity

The acquired images were analyzed with FV10-ASW software (Olympus). Regions of interest (ROIs) were placed on the nucleus region on the sensor-introduced cells, and the average fluorescence intensity of each ROI was calculated. After the average fluorescence intensity of the ROI at the region without cells was subtracted as background, the fluorescence ratio (GFP/Alexa 546) was calculated.

2.4 Results and discussion

2.4.1 FRET-Based Molecular Sensor Preparations and their Fluorescence Properties

We initially produced molecular sensors to target separate protease. We hypothesized that it would be straightforward to utilize a Fluorescence Resonance Energy Transfer (FRET) system as the sensing mechanism for proteolysis. We established chimeric FRET-based molecular sensors for varied cysteine proteases as caspase-1, 3, 9, and 14 [Kitamura et al. 2015; Suzuki et al. 2015; Suzuki et al. 2023]. Though we have already demonstrated a broad range of Alexa dyes (Alexa 532, 546, 555, 568, and 594), these combined with GFP variants could perform emission

spectrum changes upon proteolytic monitoring; there were preferable dyes for individual cysteine proteases. The structural basis for separase belonging to the cysteine protease family confirmed it to be highly homologous to caspase-9 [Lin et al. 2016], and thus we introduced Alexa 546 for our new targeted FRET-based molecular sensors because it is the optimal dye for caspase-9.

Next, we examined fluorescence emission patterns obtained upon the attachment of the dyes to two GFP variants with or without Nuclear Localization Signal (NLS), namely NLS-based and WNLS-based (without NLS), to evaluate molecular sensors regarding FRET-based sensing by FRET efficiencies of the corresponding molecular sensors (amino acid sequences are shown in Appendix 1). For each combination, significant decreases in donor fluorescence intensities and appearances of acceptor emissions were observed, as shown in Figure 2. The emission ratios were estimated as approximate FRET efficiency = donor emission intensity maximum/acceptor emission intensity maximum. The calculated FRET efficiencies of the NLS-based and WNLS-based variants were 0.164 and 0.200, respectively. In the case of commercially available protease, we can assess sensing performances as emission spectrum changes with protease treatments to obtain exchanges for FRET efficiencies; however, inaccessibility for isolated separase due to unstable behavior by dissociation from endogenous chaperone protein might prevent such operations. Therefore, tracking separase activities through live cell imaging or flow cytometric analysis could be effective for that purpose. Additionally, those high FRET efficiencies might promise to quantify separase activities in a single cell through uncomplicated data processing as emission maxima of donor molecule/emission maxima of acceptor molecule, as explained in the Section 2.

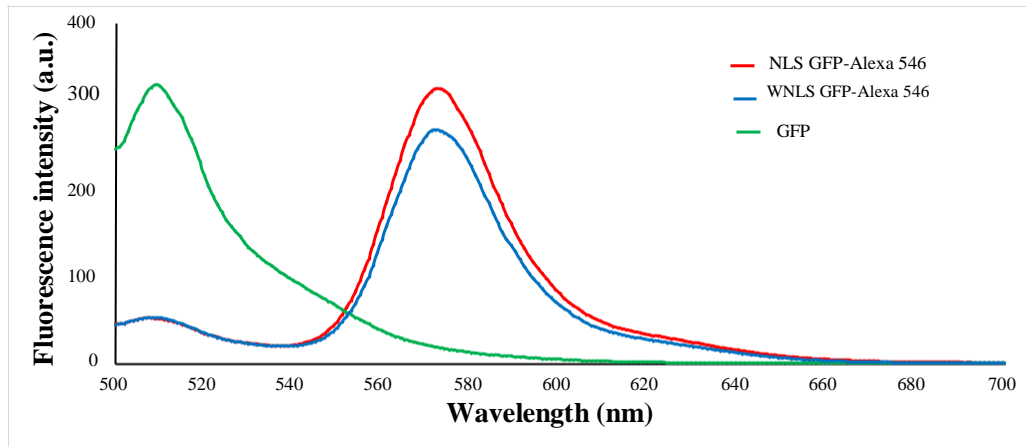


Figure 2: Emission patterns of molecular sensors excited at 488 nm. Pattern associations were shown in the inset

2.4.2 Introduction of Chimeric FRET-Based Molecular Sensors into Cell-Cycle-Controlled HeLa Cells and Flow Cytometry

After successful preparation of molecular sensors, we next assessed the molecular sensors' uptake efficiencies into HeLa cells using flow cytometry. The cell sets were subjected to donor and acceptor emission dot-plot analysis for untreated cells and treated cells in two groups: NLS GFP-Alexa 546 and WNLS GFP-Alexa 546. By gating the untreated cell populations for auto fluorescent estimation, we confirmed that more than 90% of cell populations could uptake a significant amount of the fluorescent proteins by applying a 5 μM concentration of molecular sensors. Moreover, there were no big differences between the molecular sensors analyses of the two GFP variants, as shown in Figure 3A–C.

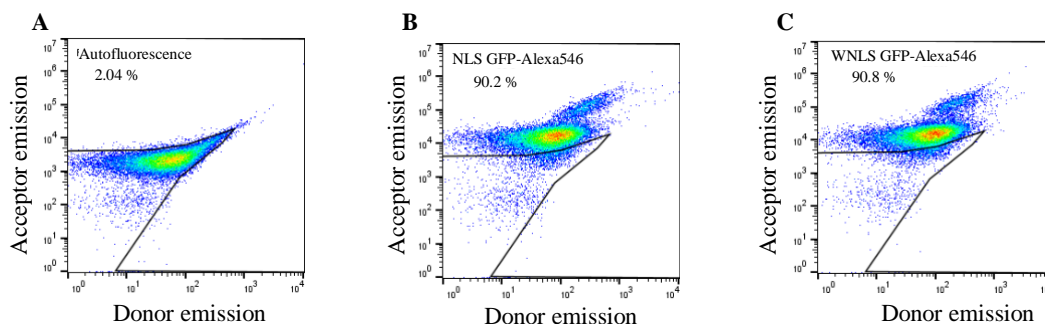


Figure 3. Flow cytometric confirmation of molecular sensors for separase-sensing uptake into HeLa cells by dot plot analysis

2.4.3 General microscopic observation of separate sensors localization inside cells

First, we observed localizations for two types of molecular sensors inside HeLa cells through the microscopic observations mentioned in Section 2.3.6. As shown in Figure 4, we obtained different distribution patterns for each molecular sensor. As for the non-localized type of molecular sensor (WNLS-based), it seemed to stay at the endosome around the nucleus to disperse into the cytosol. On the other hand, the nucleus-localized type of molecular sensor (NLS-based) accumulated inside the nucleus.

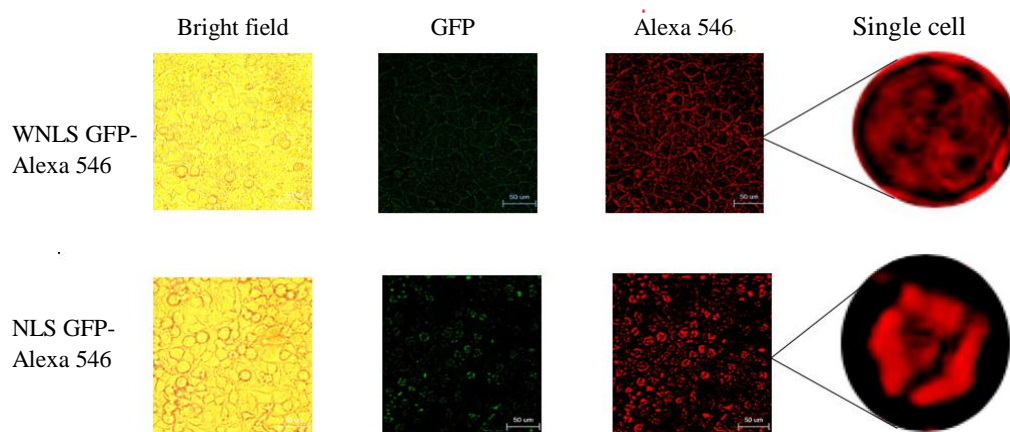


Figure 4: Fluorescence microscopic observation to compare two types of molecular sensor localizations in cells. It appeared that not localized type of molecular sensor (WNLS based) stays at endosome surrounding the nucleus to disperse into the cytosol. On the other hand, nucleus localized type of molecular sensor (NLS based) appeared to be accumulated inside nucleus.

2.4.4 Checking Cell Cycle Control/Synchronization by DNA Quantification

As separate activities in cells and proliferation rates of the cell population should correlate with the amount of DNA in the cells, we examined the influences of cell cycle synchronization by serum starvation [Chen et al. 2012] on the amount of DNA contained in the cells. HeLa cells which had undergone 48 h serum deprivation were stained with ethidium bromide and propidium iodide to compare with a non-serum-starved HeLa cell population and the DNA content was measured using a flow cytometer (SONY FACS machine). In the case of the serum starvation condition, only haploid cells were found, whereas in the cell population with the serum

supplement condition both haploid and diploid cells were observed. We thus proved that cell cycle arrest emerged as cells with haploid DNA content. Accordingly, we could collect separate-activated cells through refeeding with serum for cells.

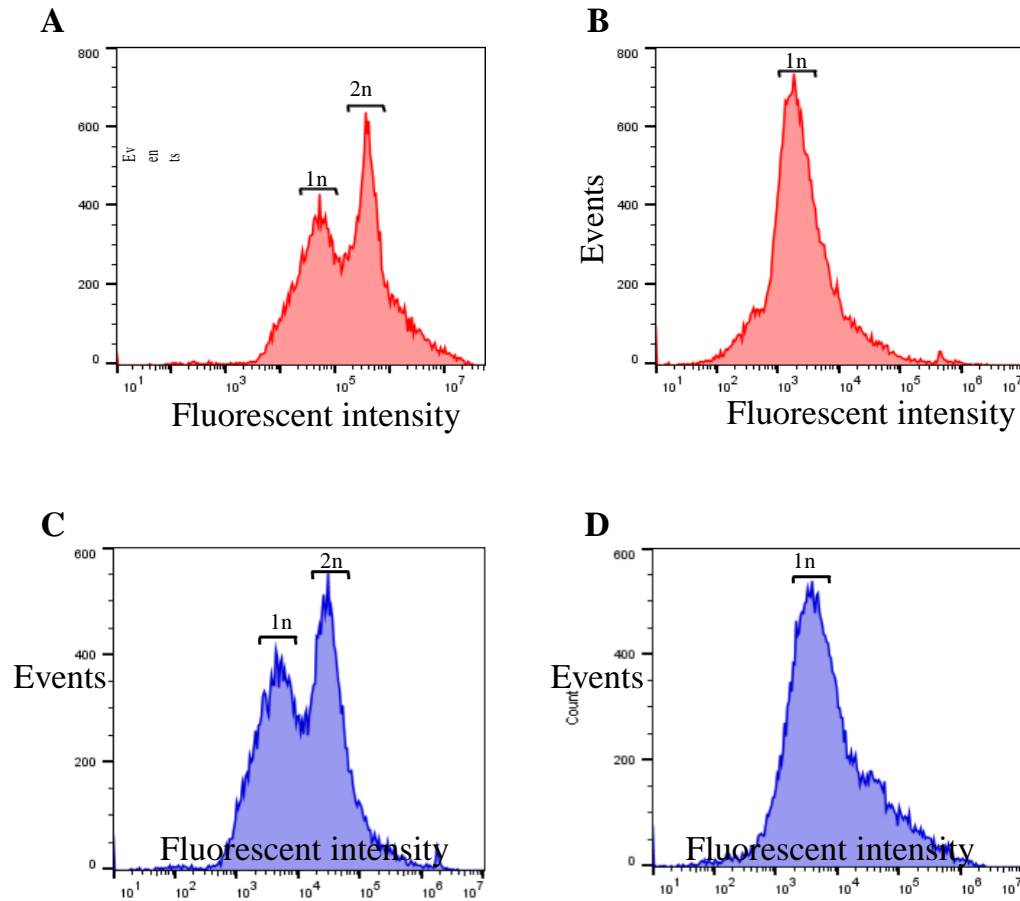


Figure 5. DNA amount in FBS-supplied (100% FBS) and FBS-starved (0% FBS) HeLa cells stained with ethidium bromide (A, B) and propidium iodide (C, D).

2.4.5 Western Blot Analysis for separase expression

We analyzed separase occurrences for cells under cell cycle control at 0 h and 24 h processing by Western blotting. As shown in Figure 6, separase occurrences in both cell populations were found. However, a more clear presence of separase was shown in the cell-lysate-derived sample that was processed for 0 h. On the other hand, the 24 h treatment indicated not only a faint

presence of separase but also several digested bands. These findings might be consistent with separase occurrences bound with the chaperone protein securin and CDK1-cyclin B1 complex to inhibit their activity before cell cycle progression and separase activation through release from those inhibitors followed by autocleavage [Konecna et al. 2023; Shindo et al. 2022]. It was reported in previous studies on human-originated separase that some autocleavable sites rendered analogous digested patterns consisting of three main bands, as a faint band at less than 150 kD, a clear band around 100 kD, and another clear band around 70 kD, during cell cycle progressions. Our band identification based on molecular markers generally matched the findings mentioned above.

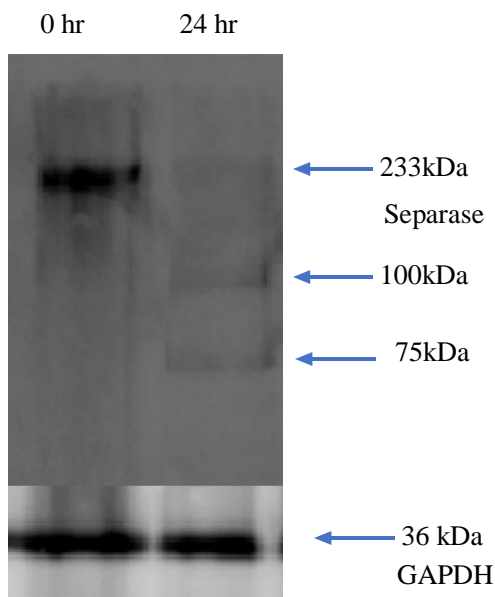


Figure 6. Separase expression profiles of cell cycle synchronized 0 h and 24 h. Blue arrow heads point to assigned bands as intact and autocleavage of separase. Comparable patterns were obtained from two more lysate preparations

2.4.6 Separase Activity Estimation Derived from Cell-Cycle-Progressed Cell Lysate

As we could obtain activated separase fractions from cell-cycle-progressed lysate preparations mentioned above, we investigated the separase activities they contained using two types of FRET-based molecular sensors. As shown in Figure 7A, we detected drastic exchanges of FRET patterns in both molecular sensors. The calculated increasing ratios of FRET efficiency were 8.70 for the NLS-based variant and 9.68 for the WNLS-based variant (Figure 7B). A slightly

more sensitive performance of separate activity detection in the lysate preparations was found in WNLS case. These results implied that constructs for the WNLS-based type could be accessible for separate with high molecular weight and were consistent with the results shown in Figure 8C.

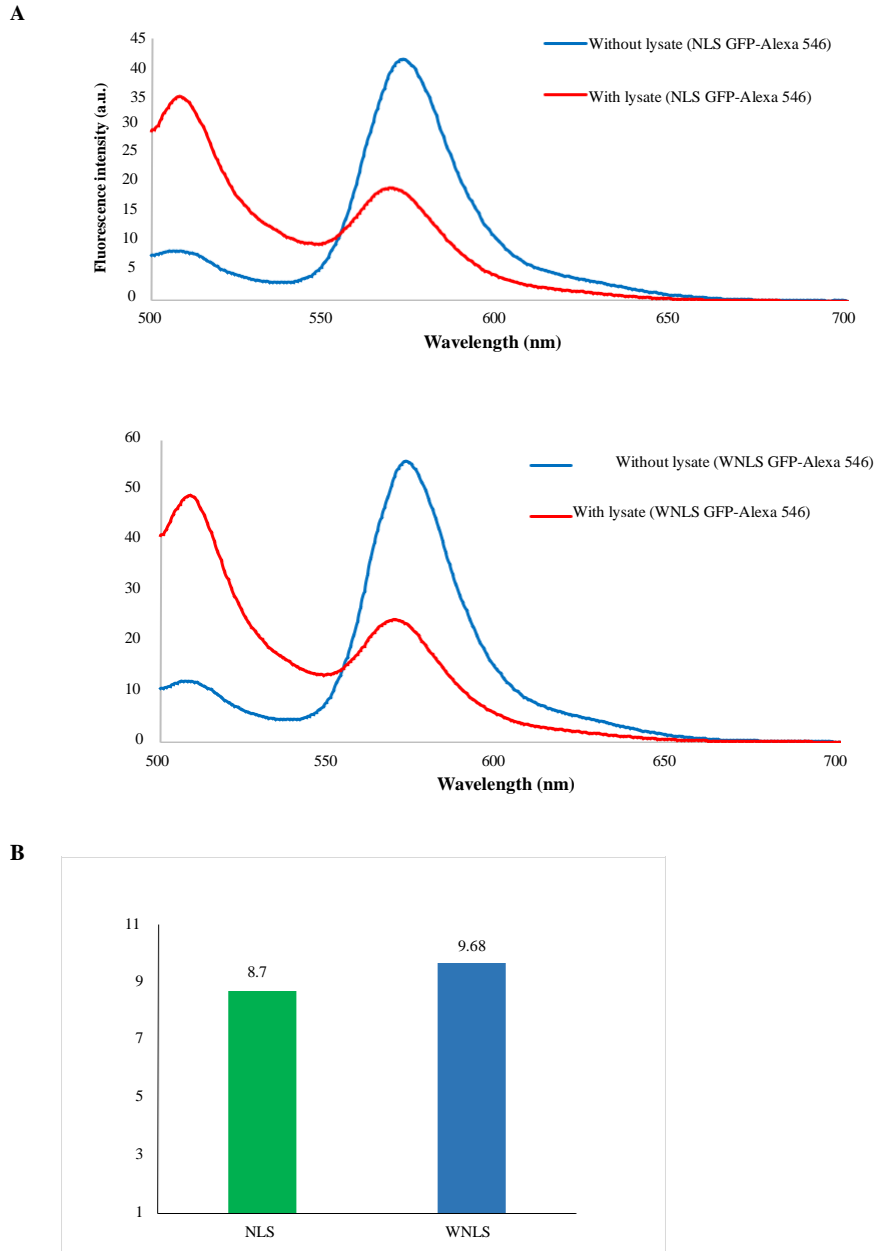


Figure 7. Separase activity validation contained in lysate preparations. (A) Emission pattern changes of molecular sensors through lysate treatments. (B) Increasing ratio of FRET efficiencies through lysate treatments

2.4.7 Separate Activations through Cell Cycle Progression

Combined with the results of our investigations into molecular sensor uptake efficiency, cell cycle synchronization by serum supplement conditions and localization of molecular sensors inside the nucleus, we next tried to monitor separate activities with molecular sensors localized inside the nucleus or dispersed in the whole cell upon separate-activated cell collection.

We measured separate activities upon cell cycle control, as shown in Figure 8A. We then checked distributions of FRET efficiencies for molecular sensors inside HeLa cells as histograms derived from populations using dot plot analysis (Figure 8B). Both cell populations demonstrated FRET efficiency increases after 24 h of re-feeding with serum. We calculated increasing ratios for 0 h to 24 h (FRET efficiencies at 24 h/FRET efficiencies at 0 h), and the calculated ratio for the NLS-based molecular sensor (1.40) was nearly the same as that for the WNLS-based one (1.42) (Figure 8C). This indicates that these molecular sensors would be adequately sensitive to detect separate activity inside cells and a sufficient amount of non-localized molecular sensor might spread to inside the nucleus.

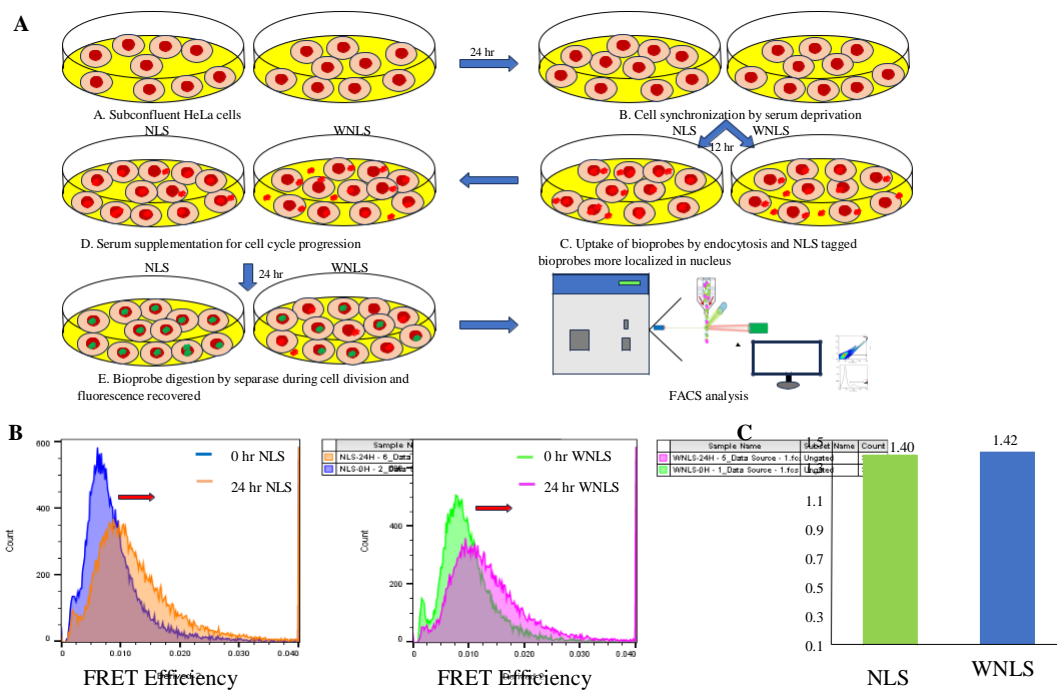


Figure 8. Separate activity monitoring through cell cycle progression. (A) Cell cycle control experimental flow was schematically drawn. (B) FRET efficiencies (after 0 h and 24 h incubation) were approximately estimated using median values from histograms for FRET

efficiencies. (C) Increasing ratios for FRET efficiencies of 0 h and 24 h were calculated for NLS- and WNLS-based molecular-sensor-introduced cell populations

2.4.8 Imaging Analysis for molecular sensor localization and separate activity

We then attempted to validate our NLS-based molecular sensor function using microscopic observations in detail upon corresponding cell cycle control. As shown in Figure 9A, it was demonstrated that the NLS-based molecular sensor almost reached the inside of the nucleus normally. Some molecular sensor uptake cells changed their shape to spherical but indicated equivalent localization patterns, as shown in Appendix 3. Though the introduction process for the molecular sensor into cells was common with flow cytometric analysis, sensitivities to fluorescence intensity were low according to microscopic observations. In previous studies, detection limits for live cell imaging were estimated around 2×10^2 for donor molecule emission and 5×10^4 for acceptor molecule emission, referring to Figure 3. Based on this estimation, an approximate average of 1% of cell populations were predicted to exceed those ranges. The percentage meeting these criteria did not render any difficulties in finding proper cells for fluorescence microscopic observations. Representative emission profiles of them are shown in Figure 9B. A small but steady increase in GFP fluorescence was observed, indicating disappearance of FRET between GFP and Alexa 546 upon digestion of the inserted separate recognition sequence. We also calculated and compared the average FRET efficiencies for cells processed for 0 h and 24 h (Figure 9C). FRET efficiency (GFP/Alexa 546) increased after cell cycle progression. These observations almost fitted with our flow cytometric analysis, i.e., our chimeric FRET-based molecular sensor could appropriately detect separate activities upon cell cycle progression.

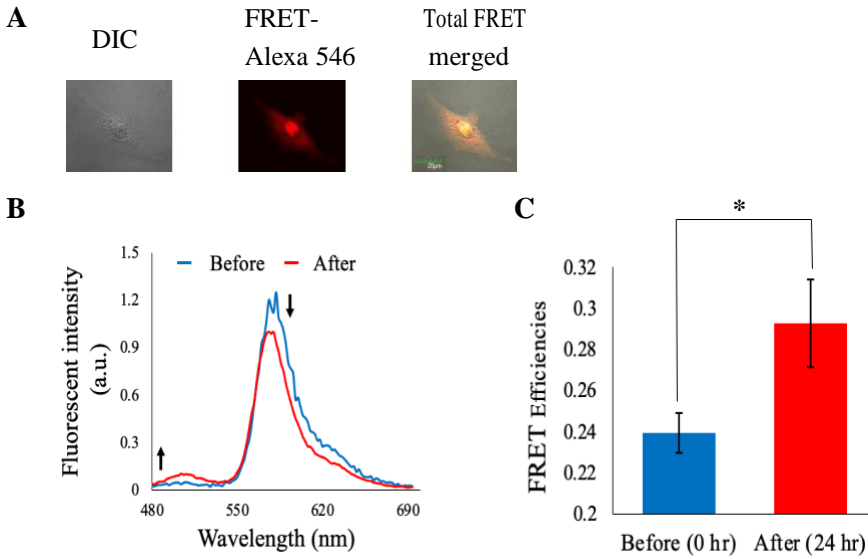


Figure 9. Separase activity monitoring through cell cycle progression. (A) Fluorescence microscopic observation of molecular sensor localization inside cells. (B) The emission profiles in HeLa cells after 0 h and 24 h incubation in culture medium containing serum. Fluorescence intensity was normalized at isosbestic point. (C) FRET efficiency exchanges before and after cell cycle progression (Before: $n = 55$ cells from three different experiments, After: 34 cells from three different experiments). Error bars: S.E.M. *: $p < 0.05$ in Student's t-test.

2.5 Conclusions

We have established live cell monitoring systems for separase activity through microscopic observation and flow cytometric analysis that could allow quantitative assay for separase activation profiles during cell cycle with spatiotemporal resolution and statistic considerations owing to consistent outcomes from both approaches. Our monitoring systems could easily be applied to other cell types [Suzuki et al. 2022]. This could render new insight for separase behaviors in live cells under cell cycle arrest or progress conditions in detail. Furthermore, our simple strategy to fabricate chimeric FRET-based molecular sensors for live cell proteolysis monitoring enables us to improve sensitivities, replace target proteases, alter localization inside cells, and change fluorescent properties by protein engineering and introductions of other combinations for fluorescent proteins and dyes. It might expand sensing targets simultaneously. Combinatorial use of molecular sensors already demonstrated for caspase-9 and -3 might straightforwardly be substituted by the sensor in this work, which would give us advanced

comprehension for separase involved in programmed cell death [Hellmuth and Stemman 2020]. In this context, we are confident that our assay will be applicable as a clinical diagnostic and prognostic tool to monitor separase proteolytic activity combined with other cellular events in human malignancies, and as a therapeutic mechanism in future studies.

Chapter III: Live cell monitoring of separase commitment to early apoptotic stage

3.1 Abstract

Separase is a key enzyme for cell division known to be categorized into cysteine protease family that initiates eukaryotic anaphase stage of mitosis during cell cycle to promote chromosome segregations through digestions of cohesin for sister chromatid cohesion. The mitotic processes include many significant physiological phenomena as cell cycle checkpoints and commitment of separase in detail have extremely been studied. On the other hand, programmed cell death is opposite but critical biological events maintain individual homeostasis in multicellular organisms. Many causes and resulting types of cell death have been linked and some members of cysteine-aspartic protease (caspases) family in most cases were identified to involve in the complex network of cell death pathways. Based on structural similarity between separase and caspase, commitment of separase to the cell death was investigated and proved to digest anti-apoptotic proteins, MCL-1 and BCL-XL. Apoptosis, typical programmed cell death are triggered by intrinsic or extrinsic stimulations and the anti-apoptotic proteins are relayed to progress early stage of intrinsic apoptotic signaling upon their digestions. In this work, we attempted to examine direct participations of separase in apoptotic networks with already developed two types of FRET-based molecular sensors for simultaneous observations of separase and apoptosis enforcement caspase (caspase-3) that exploited fluorescent proteins (donor molecule) and fluorescent dyes (acceptor molecule). We utilized flow cytometry to track their actions in living cells by anti-cancer drug treatments to stimulate intrinsic apoptotic pathways. We successfully detected separase activations upon those treatments, however, obtained still complicated signaling regulation systems.

3.2 Introduction

Live cell imaging or high-content imaging system have enthusiastically been developed for comprehensive understanding of cellular phenomena as totally different approaches with -omic studies. Especially various types and targeted molecular sensors have been exploited to monitor many biological phenomena. In some cases, more than two distinguish events were observed at a time in a single cell. However, it might still be challenge in cases of living cell population analysis for simultaneous some signaling steps, namely, high-content imaging due to elaborate sensing mechanisms. Microscopic live imaging is mostly main current.

Separase belongs to the CD clan cysteine peptidases which also includes many critical proteases for multicellular organisms is a trigger protein responsible for anaphase promotion during mitotic processes [Uhlmann et al. 2000, Mottram et al. 2012, Jeong et al. 2020]. Separase is activated at the metaphase-anaphase transition point through release from its inhibitors, securin and cyclin B, upon their degradations with "anaphase promoting complex" (APC), a ubiquitin protein ligase. Separase stimulates timely sister chromatid segregation by breaking down the cohesin protein complex, proteinaceous ring formations that entrap the chromatids together. Separase cleaves $\text{Scc1/kleisin Mcd1/Rad21}$ a subunit of the cohesin complex under temporal and spatial regulations [Uhlmann et al., 1999].

Recently some studies showed that separase can be triggered at early stage of apoptosis and direct cleavage of anti-apoptotic BCL-2 family proteins, MCL-1 and BCL-XL proteins [Hellmuth and Stemmann 2020]. The anti-apoptotic BCL-2 family proteins interact with pro-apoptotic BCL-2 family proteins, BAX/BAK under controlled interaction with their family protein, BH3 only protein [Zhang et al. 2020] to prevent them from membrane insertion, their homo-oligomerization and subsequent pore formation in mitochondrial outer membrane (MOMP). When apoptotic signals are provoked, BH3-only proteins can be activated to shift complex of BAX/BAK with their anti-apoptotic partners to homo-oligomerization by release from the anti-apoptotic proteins that might involve development for different complex of BH3 only and anti-apoptotic proteins. [Pierceall et al. 2013, Zhang et al. 2011, Zhang et al. 2020]. If active separase digests MCL-1 and BCL-XL proteins following some cellular damage occurrences, the proteolysis causes dissociation of BAK/BAX from MCL-1 and BCL-XL to facilitate series of cellular processes for MOMP related with BAK/BAX. Along with MOMP,

cytochrome c is released from mitochondria into the cytoplasm. Once released into the cytoplasm, cytochrome c connects with apoptotic peptidase activating factor-1 (APAF-1) as apoptosome, which hydrolyses procaspase 9 to generate mature caspase-9, effector caspases and the eventual induction of apoptosis (Ozoren and El-Deiry 2002).

Programmed cell death (PCD) like apoptosis and autophagy, is known as a fundamental but highly complicated biological process which conveys advantageous to multicellular living organisms by alterations of conditions for cell growth, division, and differentiation through morphological and metabolic modifications [Tang et al. 2019; Moujalled 2021; Koren et al. 2021; Jacobson et al. 1997]. The dysregulation of PCD can cause many diseases, such as Alzheimer's disease, Huntington's disease, and autoimmune disorders along with immortality of cancer cells [Cotter 2009; Nijhawan et al. 2000; Stefanis et al. 2001]. It was reported that, SEP-1 and CED-3, in *C. elegans* corresponded to separase and caspase respectively for our system, shared roles in cell division and PCD (Jeong et al 2020). There has been mounting evidence that, depending on cellular environments, cell cycle manipulations may either cause or avoid apoptotic response [Evan, 1995]. Detailed elucidation of PCD phenomena is required.

Therefore, we aimed to obtain inclusive knowledges about separase activity upon apoptosis induction and designed high-throughput and content-flow cytometric studies accompanied with some authentic approaches that exploited already developed FRET-based molecular sensors for separase and caspase-3 to detect enzymatic activity during cell cycle progress and apoptotic induction respectively. Our molecular sensors could be applied to monitor a few steps of signaling pathways simultaneously in a single cell owing to high fluorescence resolutions derived from expandable combinations of FRET pairs. Accordingly, we treated cells with anti-cancer drugs to promote mitochondria functioned apoptotic pathways under situations with only molecular sensor for caspase-3 and with molecular sensors for caspase-3 and separase together introduced into the cells to confirm apoptosis induction (the former situation) and examine separase involvement for the apoptotic pathways (the latter situation). Through flow cytometric analysis, we could obtain signals of caspase-3 activation in the former case and separase activation in the latter case, but not caspase-3 activation in the latter case. We verified that anti-cancer drug treatments resulted in time dependent progress of apoptosis by microscopic

observations. Additionally, more progressed apoptosis appeared to occur under situations without any molecular sensors upon anti-cancer drug treatments. This observation might render separate activation occurrences upon mitochondria related apoptotic pathway stimulations to digest anti-apoptotic BCL-2 family proteins (MCL-1 and BCL-XL) and promote further apoptotic pathways, however, competition for separate with molecular sensors for separate and MCL-1 and BCL-XL to cause insufficient promotion of the later stage of apoptotic pathways. Our results demonstrated the separate commitment to progress of early apoptotic stage. Though this hypothesis should carefully be assessed more, we showed first evidence for activation of separate upon apoptotic inductions with live monitoring approaches in this study.

3.3 Materials and methods

3.3.1 Fluorescent Protein Isolations

Three types of fluorescent protein mutants; two green fluorescent protein (GFP) and one red fluorescent protein (RFP) were isolated and validated as previously described. Briefly, previously prepared plasmids encoding GFP derivatives inserted recognition sequences of separate, DREIMRE (pUV5Sep) or caspase-3, DEVD (pUV5casS52tag) and RFP derivative inserted recognition sequence of caspase-3, DEVD (pT3castag) were transfected into *Escherichia coli* BL21 cells (DE3). The transfected bacteria were cultured in Luria Bertani (LB) medium containing 75 µg/ml of ampicillin; the expression of the GFP and RFP derivatives were induced by isopropyl-β-D-thiogalactopyranoside (IPTG). The bacteria were harvested and lysed with enough amount of bacterial protein extraction reagent, B-PER II (Thermo Scientific Pierce, Rockford, IL, USA). The target proteins were isolated from the lysate by centrifugation for separation from cell debris and purified using Ni²⁺-NTA (nitrilotriacetic acid) affinity chromatography through (Histidine)₆ tag sequence fused with GFP and RFP derivatives. The remaining reagents were removed with gel filtration column and recovered proteins were then reconstituted in phosphate buffered saline (PBS).

3.3.2 FRET-based molecular sensor preparations

Isolated fluorescent proteins mentioned above were chemically modified with already established methods. Two types of fluorescent dyes such as Alexa Fluor-546 for both GFP mutants and Alexa Fluor-647 for the RFP mutant (Life Technologies, Carlsbad, CA, USA) (Thermo Scientific Pierce). 10 μ M of GFP and RFP mutants dissolved in PBS were reduced with 1mM of dithiothreitol (DTT) for 10 minutes at room temperature. Excess DTT was removed by gel filtration equilibrated with PBS (NICK column, GE Healthcare, Buckinghamshire, UK), and an aliquot of the eluate was immediately incubated with the applicable fluorescent dye in dimethyl sulfoxide (DMSO) at the molar ratio of 1:10 at 37 °C for 4 h followed to stand for at 4 °C for 6 h. The resulting solution was subjected to centrifugal filtration with Amicon Ultra-0.5 Ultracel 10 (EMD, Millipore, Billerica, MA, USA) to remove any unreacted dye and concentrate it to an appropriate volume for use in subsequent analyses. The FRET-based molecular sensors were assessed by fluorescence spectroscopy using a Shimadzu RF-5300PC spectrophotometer (Shimadzu, Kyoto, Japan) excited at 488 nm and 565 nm (GFP and RFP excitation) respectively.

3.3.3 FRET-based molecular sensor digestions with caspase-3 *in vitro*

We verified obtained FRET-based molecular sensors for caspase-3 activity detection and specificity *in vitro* using determined approaches. In short, 1.0 unit of caspase-3 was added to 20 μ L of 2 μ M chemically derivatized two GFP mutants with Alexa Fluor 546 and one RFP mutant with Alexa Fluor 647 dyes reconstituted in caspase assay buffer containing 20 mM 2-[4-(2-sulfoethyl) piperazin-1-ium-1-yl] ethanesulfonate (PIPES), 100 mM NaCl, 0.1% 3-[dimethyl(3- $\{[(3\alpha,5\beta,7\alpha,12\alpha)-3,7,12\text{-trihydroxy-24-oxocholan-24yl]amino\}$ propyl) ammonio] propane-1-sulfonate (CHAPS), 10 mM DTT, 10% sucrose, and 1 mM EDTA. The mixture was then incubated for 2 h at 37 °C. We also prepared a corresponding sample without caspase-3 addition as a control. Fluorescence spectra for all the samples were measured equally deduce the FRET efficiency exchanges compared with a pair of FRET efficiencies.

3.3.4 Introduction of chimeric FRET bioprobes into HeLa cells

FRET-based molecular sensor was confirmed to be introduced into cells through straightforward methods by the incubation of cells with culture media including molecular sensors. Cell types

and culture media are almost unlimited. Subcultured HeLa cells were seeded into 24 wells plate filled with adequate amount of Dulbecco's Modified Eagle Medium (DMEM) supplied with 10% fetal bovine serum (FBS) and cultured at 37°C under an atmosphere containing 5% CO₂. After confirmation of confluency of cells with microscopy, the culture medium was replaced with fresh 600 µl of DMEM without FBS including 5µM of FRET-based molecular sensors (GFP after washing the cells with fresh DMEM without FBS several times. Then, the cells were incubated at 37°C under an atmosphere containing 5% CO₂ for 24 hrs. The culture media was refreshed with DMEM supplied with 10% FBS and the resulting cells were subjected to further experiments.

3.3.5 Induction of intrinsic apoptosis with anti-cancer drugs to HeLa cells

HeLa cells introduced only FRET-based molecular sensor, dye attached RFP derivative for caspase-3 activity detection and combination of the RFP derivative and dye attached GFP derivative for separase activity detection were treated with final concentration as 10µM of Docetaxel and (100 mg/ml) of 4-((2R)-2-((1S,3S,5S)-3,5-dimethyl-2-oxocyclohexyl)-2-hydroxyethyl) piperidine-2,6-dione (cycloheximide). Appropriate amount DMSO was applied to HeLa cells to examine solvent affects to the cells. The treated cells were incubated for 24 h before microscopic observations and flow cytometric analysis.

3.3.6 Microscopic observation of HeLa cells upon apoptosis induction

Approximate investigations of apoptotic induction stages were carried out by microscopic observations with bright field after treatment of anti-cancer drugs at room temperature using an ECLIPSE TE 2000U (Nikon Solutions Co., Ltd., Tokyo, Japan) with a ×40 water immersion objective lens.

3.4 Results and discussion

3.4.1 Preparation of molecular sensors and sensing evaluation in *in vitro*

We produced three molecular sensors targeting for separase and caspase-3. We proposed that a Fluorescence Resonance Energy Transfer (FRET) system might be easily employed as the sensing approach for proteolysis. The responsiveness of six combinations of molecular sensors to

caspase-3 was examined by means of fluorescence spectroscopy. Significant changes in the emission profiles upon treatment with caspase-3 were observed, and typical pattern changes were found at caspase-3 sensing GFP based molecular sensor. But Separase sensor has shown no emission pattern changes upon caspase-3 treatment that means no digestion upon caspase-3 treatment. Very few characteristic pattern alterations were seen when caspase-3 was treated in the RFP-based caspase-3 molecular sensor. We calculated the emission ratio (fluorescent protein emission maximum/ dye emission maximum) in the presence and absence of caspase-3 (Figure 10 (A) and (B)). We then approximated changes in the ratio of the emission ratio with caspase-3 to that of the emission ratio without caspase-3 (Table1). However, We, already established RFP-Alexa Flour 647 sensor and highly sensitive to caspase-3 (Suzuki et al. 2012). Calculated FRET efficiencies and exchange ratios of them were listed in Table 1.

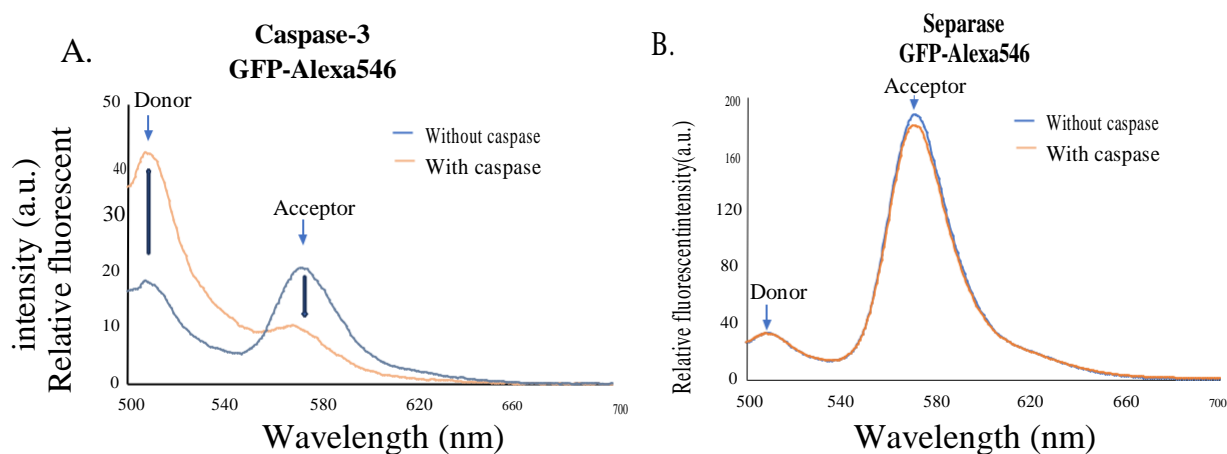


Figure 10. Changes in the emission patterns of molecular sensors at *in vitro* treatment with caspase-3 for GFP-based caspase-3 molecular sensor (A) and separase sensor (B) (Caspase-3 presence (orange) or absence (blue)).

	FRET Efficiency	Exchange ratio
Separase-Alexa546		
Without caspase	0.182	1.02
With caspase	0.177	
Caspase3-Alexa647		
Without caspase	10.41	1.36
With caspase	7.65	

Table 1: Emission ratios of FRET-based GFP and RFP molecular sensors for separate and caspase-3 sensing

3.4.2 Single use molecular sensor for caspase-3 activities upon apoptotic induction in HeLa cells by flow cytometric analysis

After successfully preparation of RFP based molecular sensor, we introduced in HeLa cells and checked the activity of caspase-3 with anticancer drug treatments. First, we assessed molecular sensor uptake efficiencies into HeLa cells using flow cytometry. By gating of autofluorescent cell population, we confirmed that a significant amount of the molecular sensors was introduced into HeLa cells. We observed differences in distributions of populations against x axis (Donor emission) and y axis (Acceptor emission). So, we could adequately detect FRET efficiencies using flow cytometric analysis. We then checked distributions of FRET efficiencies for molecular sensors digestion inside HeLa cells as histograms derived from population distributions shown in dot plot. The peak values in histograms for apoptosis-induced cells were shifted to smaller values at right side in comparison those of nontreated anti cancer drug treatments, showing that increases in the emission ratio occur as a result of cancelation of FRET (Figure 11). As in case of sensing of protease activities, FRET would be suppressed to produce molecular sensor with lower acceptor emission and higher donor emission. These observations show that our FRET-based RFP sensor is capable of sensing caspase-3 activation inside HeLa cells. In this experiment, DMSO was applied to examine solvent affects to the cells.

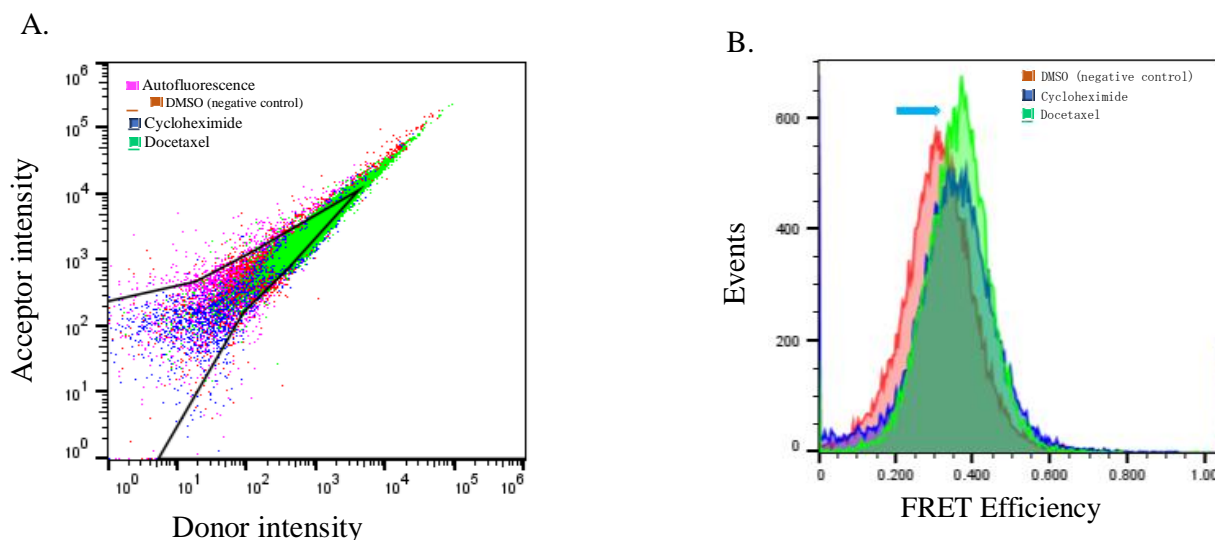


Figure 11. Uptake efficiency of Chimeric FRET-Based caspase-3 sensing RFP sensor into Cell-Cycle-Controlled HeLa Cells (A) and FRET efficiencies were estimated using histograms with anti-cancer drug treatments (B) by flow cytometry.

3.4.3 Double use molecular sensors for separase and caspase-3 activities upon apoptosis induction by Flow cytometric analysis

After confirmation of RFP-Alexa Fluor647 molecular sensor digestion upon caspase-3 inside HeLa cells with anticancer drug treatments then we try to introduce both GFP-Alexa546 and RFP-Alexa647 sensors in a population for detecting the activity of separase and caspase-3 simultaneously in HeLa cells upon apoptosis induction. Next, we used flow cytometry to evaluate the molecular sensor absorption efficiency into HeLa cells. We verified that both molecular sensors were incorporated into a considerable quantity in HeLa cells by gating the population of autofluorescent cells. We observed differences in distributions of populations against x axis (Donor emission) and y axis (Acceptor emission). We then checked distributions of FRET efficiencies as histograms derived from population distributions shown in dot plot. Results shows that GFP based sensor only digested but RFP based sensor not digested (Figure 12 (B) and (D)). That indicated that separase is active upon digestion of sensor but caspase-3 not active upon apoptosis induction. We consider separase is active at early apoptotic stage and digest of antiapoptotic BCL-XL and MCL-1 proteins as well as molecular sensor simultaneously. So, Separase need to compete with molecular sensors for separase and (MCL-1, BCL-XL) anti apoptotic proteins so insufficient promotion of later stage of apoptotic pathways. When apoptotic progression reduced and Caspase-3 not digest RFP based sensor. In this experiment, DMSO was applied to examine solvent affects to the cells.

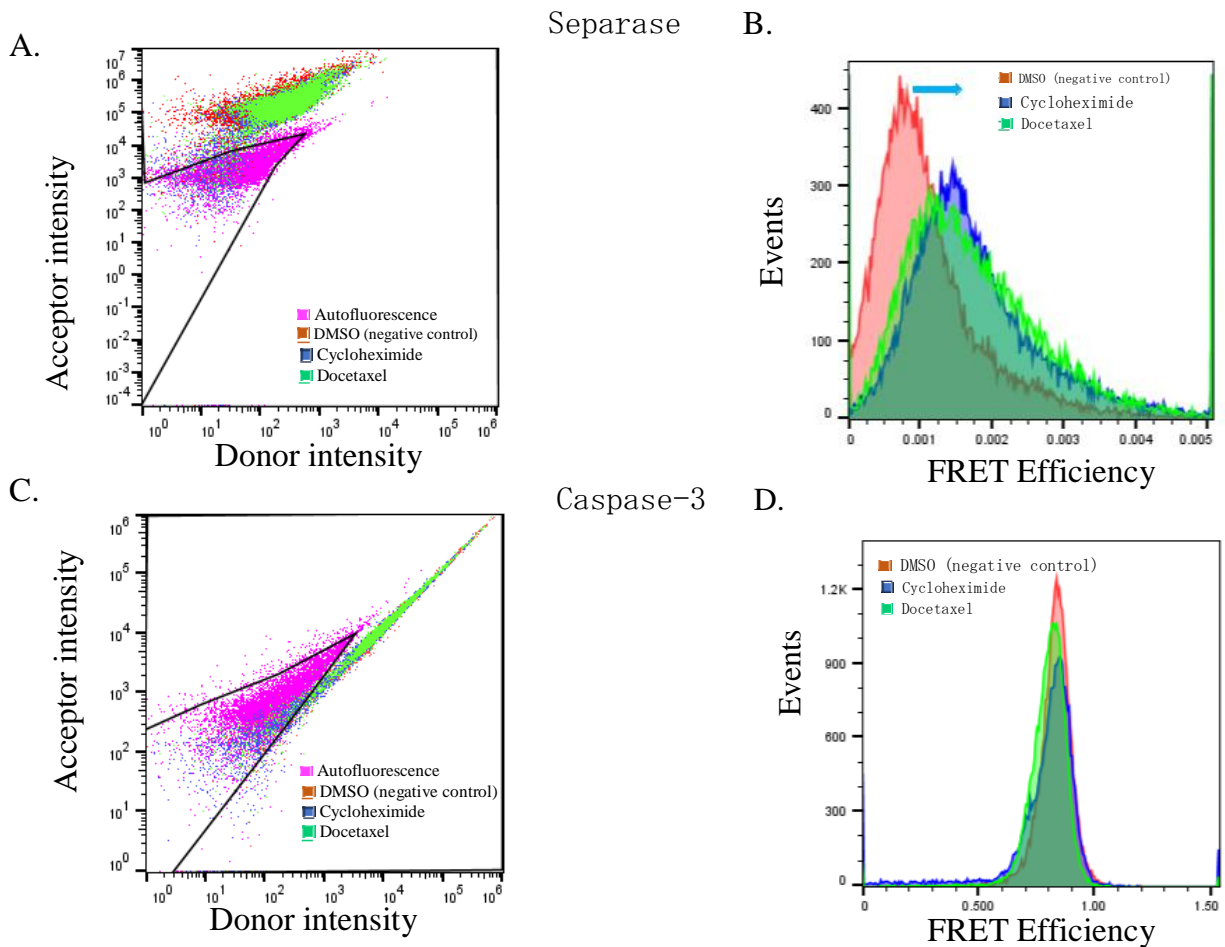


Figure12. Uptake efficiency of Chimeric FRET-Based GFP and RFP based molecular sensors for separase and caspase-3 sensing into Cell-Cycle-Controlled HeLa Cells. (A and C) and FRET efficiencies were estimated using histograms with anti-cancer drug treatments by flow Cytometry (B and D).

3.4.4 Microscopic observation of HeLa cells upon apoptosis induction

Several apoptotic induction phases after treatment with anticancer drugs observed by bright field microscopic analysis at room temperature. We verified that anti-cancer drug treatments resulted in time dependent progress of apoptosis by microscopic observations. We observed apoptotic progression at 24 and 48 hours with molecular sensors introduction and 24 hours without molecular sensors introduction. More advanced apoptosis seemed to happen in the presence of

no molecular sensors during anti-cancer medication treatments after 24 hours. After 24 hours, the application of two anticancer drugs demonstrated more progress than that of one. However, the state was more advanced after 48 hours with the molecular sensor. The sequential apoptotic progression is as follows: 24H Bioprobe < 24H No Bioprobe < 24H No Bioprobe+ TNF- α < 48H Bioprobe. This results consistent with the flow cytometry experimental data.

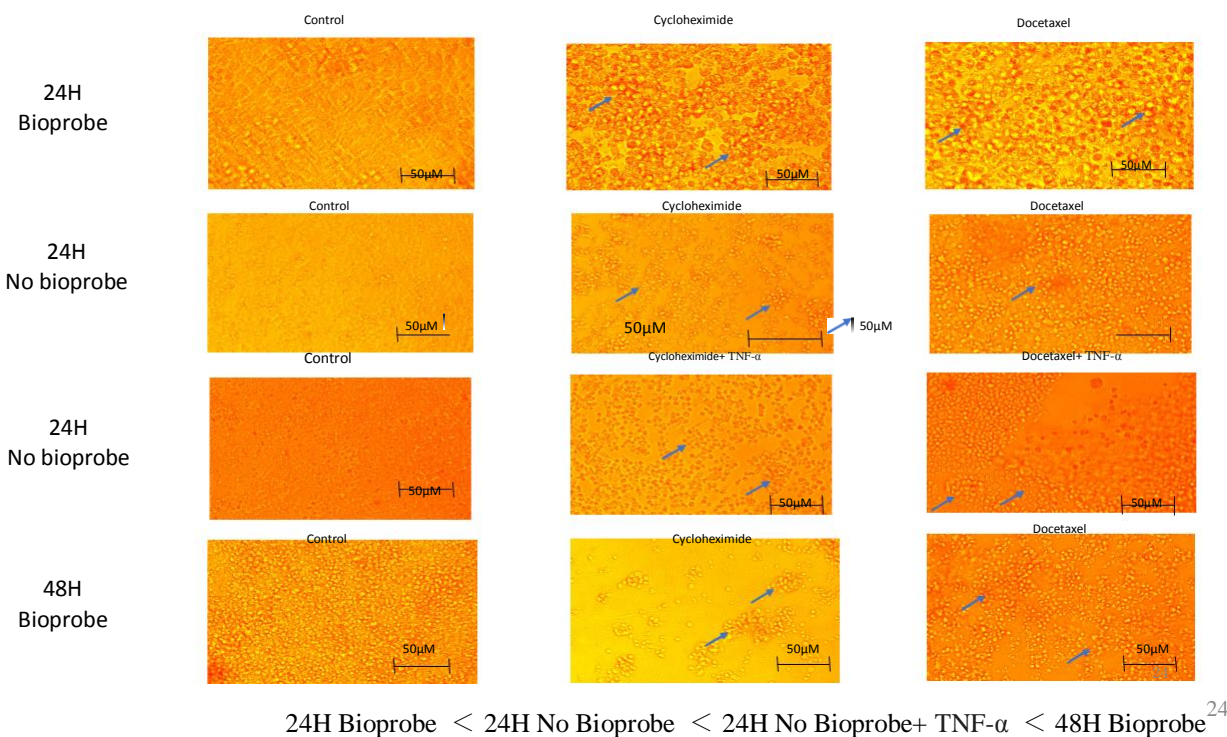


Figure 13. Microscopic observation of HeLa cells in the presence and absence of molecular sensors with anticancer drug treatments

3.5 Conclusions

In summary, we used straightforward approaches to make three sets of FRET-based chimeric molecular sensors for two types of proteases as separase and caspase-3. We successfully detected activation of separase with live monitoring approaches upon apoptotic inductions. Our results demonstrated the separase commitment to progress of early apoptotic stage upon anti-cancer drug treatments though this hypothesis should carefully be assessed more in future. We could further improve the intrinsic sensitivities of our bioprobes by development of the various components and their linkages; concentration of molecular sensors and selectivity of anti cancer

drugs, longevity of drug induction, and sensitivities of molecular sensors could be improved by optimization of the amounts with cell cycle progression. These improvements might result in a much more informative sensing system for programmed cell death as well as cell cycle progression.

References

Agarwal, R.; Cohen-Fix, O. Phosphorylation of the mitotic regulator Pds1/securin by Cdc28 is required for efficient nuclear localization of Esp1/separase. *Genes Dev.* **2002**, *16*, 1371–1382.

Alnemri, T.F.; Armstrong, R.C.; Krebs, J.; Srinivasula, S.M.; Wang, L.; Bullrich, F.; Fritz, L.C.; Trapani, J.A.; Tomaselli, K.J.; Litwack, G.; et al. In vitro activation of CPP32 and Mch3 by Mch4, a novel human apoptotic cysteine protease containing two FADD-like domains. *Proc. Natl. Acad. Sci. USA* **1996**, *93*, 7464–7469.

Baskerville, C.; Segal, M.; Reed, S.I. The protease activity of yeast separase (esp1) is required for anaphase spindle elongation independently of its role in cleavage of cohesin. *Genetics* **2008**, *178*, 2361–2372.

Boland, A.; Martin, T.G.; Zhang, Z.; Yang, J.; Bai, X.C.; Chang, L.; Scheres, S.H.; Barford, D. Cryo-EM structure of a metazoan separase-securin complex at near-atomic resolution. *Nat. Struct. Mol. Biol.* **2017**, *24*, 414–418.

Buonomo, S.B.C.; Clyne, R.K.; Fuchs, J.; Loidl, J.; Uhlmann, F.; Nasmyth, K. Disjunction of homologous chromosomes in meiosis I depends on proteolytic cleavage of the meiotic cohesin Rec8 by separin. *Cell* **2000**, *103*, 387–398.

Chen, M.; Huang, J.; Yang, X.; Liu, B.; Zhang, W.; Huang, L. Serum Starvation Induced Cell Cycle Synchronization Facilitates Human Somatic Cells Reprogramming. *PLoS ONE* **2012**, *7*, e28203.

Chestukhin, A.; Pfeffer, C.; Milligan, S.; DeCaprio, J.A.; Pellman, D. Processing, localization, and requirement of human separase for normal anaphase progression. *Proc. Natl. Acad. Sci. USA* **2003**, *100*, 4574–4579.

Ciosk, R.; Zachariae, W.; Michaelis, C.; Shevchenko, A.; Mann, M.; Nasmyth, K. An ESP1/PDS1 complex regulates loss of sister chromatid cohesion at the metaphase to anaphase transition in yeast. *Cell* **1998**, *93*, 1067–1076.

Cohen-Fix, O.; Peters, J.M.; Kirschner, M.W.; Koshland, D. Anaphase initiation in *Saccharomyces cerevisiae* is controlled by the APC-dependent degradation of the anaphase inhibitor Pds1p. *Genes Dev.* **1996**, *10*, 3081–3093.

Cotter, T.G. Apoptosis and cancer: The genesis of a research field. *Nat. Rev. Cancer.* **2009**, 501–507.

Csizmok, V.; Felli, I.C.; Tompa, P.; Banci, L.; Bertini, I. Structural and dynamic characterization of intrinsically disordered human securin by NMR spectroscopy. *J. Am. Chem. Soc.* **2008**, *130*, 16873–16879.

Diana, P.; Elisa, G.; Konstantinos, L.; Tullio, P. Exploring cells with targeted biosensors. *J. Gen. Physiol.* **2017**, *149(1)*, 1–36.

Elmore, S. Apoptosis: a review of programmed cell death. *Toxicol. Pathol.* **2007**, *35*, 495–516.

Evan, G.I.; Brown, L.; Whyte, M.; Harrington, E; Apoptosis and the cell cycle. *Curr Opin Cell Biol.* **1995**, *7*, 825-34.

Funabiki, H.; Kumada, K.; Yanagida, M. Fission yeast Cut1 and Cut2 are essential for sister chromatid separation, concentrate along the metaphase spindle and form large complexes. *EMBO J.* **1996**, *15*, 6617–6628.

Galluzzi, L.; Vitale, I.; Aaronson, S. A.; Abrams, J. M.; Adam, D.; Agostinis, P. (2018). Molecular mechanisms of cell death: recommendations of the nomenclature committee on cell death 2018. *Cell Death Differ.* **2007**, *25*, 486–541.

Gorr, I.H.; Boos, D.; Stemmann, O. Mutual inhibition of separase and Cdk1 by two-step complex formation. *Molecular Cell* **2005**, *19*, 135–141.

Hauf, S.; Waizenegger, I.C.; Peters, J.M. Cohesin cleavage by separase required for anaphase and cytokinesis in human cells. *Science* **2001**, *293*, 1320–1323.

Hellmuth, S.; Böttger, F.; Pan, C.; Mann, M.; Stemmann, O. PP2A delays APC/C-dependent degradation of separase-associated but not free securin. *EMBO J.* **2014**, *33*, 1134–1147.

Hellmuth, S.; Gutiérrez-Caballero, C.; Llano, E.; Pendás, A.M.; Stemmann, O. Local activation of mammalian separase in inter- phase promotes double-strand break repair and prevents oncogenic transformation. *EMBO J.* **2018**, *37*, e99184.

Hellmuth, S.; Rata, S.; Brown, A.; Heidmann, S.; Novak, B.; Stemmann, O. Human chromosome segregation involves multi-layered regulation of separase by the peptidyl-prolyl-isomerase Pin1. *Mol. Cell* **2015**, *58*, 495–506.

Hellmuth, S.; Stemman, O. Separase-triggered apoptosis enforces minimal length mitosis. *Nature* **2020**, *580*, 542–547.

Henschke, L.; Frese, M.; Hellmuth, S.; Marx, A.; Stemmann, O.; Mayer, T.U. Identification of Bioactive Small Molecule Inhibitors of Separase. *ACS Chem. Biol.* **2019**, *14*, 2155–2159.

Herzig, A.; Lehner, C.F.; Heidmann, S. Proteolytic cleavage of the THR subunit during anaphase limits Drosophila separase function. *Genes Dev.* **2002**, *16*, 2443–2454.

Holland, A.J.; Böttger, F.; Stemmann, O.; Taylor, S.S. Protein phosphatase 2A and separase form a complex regulated by separase autocleavage. *J. Biol. Chem.* **2007**, *282*, 24623–24632.

Hornig, N.C.; Knowles, P.P.; McDonald, N.Q.; Uhlmann, F. The dual mechanism of separase regulation by securin. *Curr. Biol.* **2002**, *12*, 973–982.

Imai, Y.; Matsushima, Y.; Sugimura, T.; Terada, M. A simple and rapid method for generating a deletion by PCR. *Nucleic Acids Res.* **1991**, *19*, 2785.

Jackson, S.P.; Bartek, J. The DNA-damage response in human biology and disease. *Nature* **2009**, *461*, 1071–1078.

Jacobson, M.D., Weil, M. and Raff, M.C. Programmed cell death in animal development. *Cell.* **1997**, *88*, 347–354

Jallepalli, P.V.; Lengauer, C. Chromosome segregation and cancer: Cutting through the mystery. *Nat. Rev. Cancer* **2001**, *1*, 109–117.

Jeong, P.Y.; Kumar, A.; Joshi, P.M.; Rothman, J.H. Intertwined Functions of Separase and Caspase in Cell Division and Programmed Cell Death. *Sci Rep.* **2020**, *10*(1), 6159. doi: 10.1038/s41598-020-63081-w. PMID: 32273538; PMCID: PMC7145830.

Kalderon, D.; Roberts, B.L.; Richardson, W.D.; Smith, A.E. A short amino acid sequence able to specify nuclear location. *Cell* **1984**, *39*, 499–509.

Kitamura, A.; Nakayama, Y.; Kinjo, M. Efficient and dynamic nuclear localization of green fluorescent protein via RNA binding. *Biochem. Biophys. Res. Commun.* **2015**, *463*, 401–406.

Konecna, M.; Abbasi Sani, S.; Anger, M. Separase and Roads to Disengage Sister Chromatids during Anaphase. *Int. J. Mol. Sci.* **2023**, *24*, 4604.

Koren, E. Fuchs, Y. Modes of Regulated Cell Death in Cancer. *Cancer Discov.* **2021**, *11*, 245–265.

Lee, K.; Rhee, K. Separase-dependent cleavage of pericentrin B is necessary and sufficient for centriole disengagement during mitosis. *Cell Cycle* **2012**, *11*, 2476–2485.

Lin, Z.; Luo, X.; Yu, H. Structural basis of cohesin cleavage by separase. *Nature* **2016**, *532*, 131–134.

Luo, S.; Tong, L. Molecular mechanism for the regulation of yeast separase by securin. *Nature* **2017**, *542*, 255–259.

Matsuo, K.; Ohsumi, K.; Iwabuchi, M.; Kawamata, T.; Ono, Y.; Takahashi, M. Kendrin is a novel substrate for separase involved in the licensing of centriole duplication. *Curr. Biol.* **2012**, *22*, 915–921.

McAleenan, A.; Clemente-Blanco, A.; Cordon-Preciado, V.; Sen, N.; Esteras, M.; Jarmuz, A.; Aragón, L. Post-replicative repair involves separase-dependent removal of the kleisin subunit of cohesin. *Nature* **2013**, *493*, 250–254.

McIlwain, D.R., Thorsten, B., Mak, T.W. (2013). Caspase Functions in Cell Death and Disease Cold Spring Harb. *Perspect Biol.* **2013**, *5*(4): a008656

Moujalled, D.; Strasser, A., Liddell, J.R. Molecular mechanisms of cell death in neurological diseases. *Cell Death Differ* **2021**, *28*, 2029–2044.

Mottram, J. C.; Helms, M.J.; Coombs, G.H.; Sajid, M. Clan CD cysteine peptidases of parasitic protozoa. *Trends Parasitol* **2003**, *19*, 182–187.

Nagao, K.; Adachi, Y.; Yanagida, M. Separase-mediated cleavage of cohesin at interphase is required for DNA repair. *Nature* **2004**, *430*, 1044–1048.

Nakamura, A.; Arai, H.; Fujita, N. Centrosomal Aki1 and cohesin function in separase-regulated centriole disengagement. *J. Cell Biol.* **2009**, *187*, 607–614.

Nijhawan, D.; Honarpour, N. and Wang, X. Apoptosis in neural development and disease. *Annu Rev Neurosci.* **2000**, *23*, 73–87.

Nirmala, J. G., and Lopus, M. Cell death mechanisms in eukaryotes. *Cell Biol. Toxicol.* **2020**, *36*, 145–164.

Oliveira, R.A., and Nasmyth, K. Getting through anaphase: splitting the sisters and beyond. *Biochem. Soc. Trans.* **2010**, *38*, 1639–1644.

Oliveira, R.A., Hamilton, R.S., Pauli, A., Davis, I., and Nasmyth, K. Cohesin cleavage and Cdk inhibition trigger formation of daughter nuclei. *Nat. Cell Biol.* **2010**, *12*, 185–192.

Ozoren, N.; El-Deiry, W.S. Defining characteristics of types I and II apoptotic cells in response to TRAIL. *Neoplasia* (New York, NY). **2002**, *4*, 551–7.

Papi, M.; Berdugo, E.; Randall, C.L.; Ganguly, S.; Jallepalli, P.V. Multiple roles for separase auto-cleavage during the G2/M transition. *Nat. Cell Biol.* **2005**, *7*, 1029–1035.

Peters, J.-M. The anaphase-promoting complex: Proteolysis in mitosis and beyond. *Mol. Cell* **2002**, *9*, 931–943.

Pierceall W.E.; Kornblau, S.M.; Carlson, N.E.; Huang, X.; Blake, N.; Lena, R.; Elashoff, M.; Konopleva M; Cardone M.H.; Andreeff, M. BH3 Profiling Discriminates Response to Cytarabine-Based Treatment of Acute Myelogenous Leukemia. *Mol. Cancer Ther.* **2013**, *12*, 2940–2949.

Rao, H.; Uhlmann, F.; Nasmyth, K.; Varshavsky, A. Degradation of a cohesin subunit by the N-end rule pathway is essential for chromosome stability. *Nature* **2001**, *410*, 955–959.

Rogers, G.C.; Rogers, S.L.; Schwimmer, T.A.; Ems-McClung, S.C.; Walczak, C.E.; Vale, R.D.; Scholey, J.M. and Sharp, D.J. Two mitotic kinesins cooperate to drive sister chromatid separation during anaphase. *Nature*. **2004**, *427*, 364–370.

Sanchez-Puig, N.; Veprintsev, D.B.; Fersht, A.R. Human full-length Securin is a natively unfolded protein. *Protein Sci.* **2005**, *14*, 1410–1418.

Schockel, L.; Mockel, M.; Mayer, B.; Boos, D.; Stemmann, O. Cleavage of cohesin rings coordinates the separation of centrioles and chromatids. *Nat. Cell Biol.* **2011**, *13*, 966–972.

Schultz, C.; Schleifenbaum, A.; Goedhart, J. and Gadella, T. W., Jr. Multiparameter imaging for the analysis of intracellular signaling, *Chembiochem.* **2005**, *6*, 1323–1330

Shindo, N.; Kumada, K.; Iemura, K.; Yasuda, J.; Fujimori, H.; Mochizuki, M.; Tamai, K.; Tanaka, K.; Hirota, T. Autocleavage of separase suppresses its premature activation by promoting binding to cyclin B1. *Cell Rep.* **2022**, *41*, 111723.

Stefanis, L., and Rideout, H. Caspase inhibition: a potential therapeutic strategy in neurological diseases. *Histol. Histopathol.* **2001**, *16*, 895– 908

Suzuki, M.; Sakata, I.; Sakai, T.; Tomioka, H.; Nishigaki, K.; Tramier, M.; Coppey-Moisan, M. A high-throughput direct fluorescence resonance energy transfer-based assay for analyzing apoptotic proteases using flow cytometry and fluorescence lifetime measurements. *Anal. Biochem.* **2015**, *291*, 10–17.

Suzuki, M.; Shindo, Y.; Yamanaka, R.; Oka, K. Live imaging of apoptotic signaling flow using tunable combinatorial FRET-based bioprobes for cell population analysis of caspase cascades. *Sci. Rep.* **2022**, *12*, 21160.

Suzuki, M.; Taguma, K.; Bandaranayake, U.K.; Ikeda, W. Development of Ratiometric Fluorescence Sensing Molecule for Caspase-14, a Key Enzyme of Epidermis Metabolism. *J. Biomed. Res. Environ. Sci.* **2023**, *4*, 793–800.

Suzuki, M.; Tanaka, S.; Ito, Y.; Inoue, M.; Sakai, T.; Nishigaki, K. Simple and tunable Förster resonance energy transfer-based bioprobes for high-throughput monitoring of caspase-3 activation in living cells by using flow cytometry. *Biochem. Biophys. Acta.* **2012**, *1823*, 215–226.

Tang, D.; Kang, R.; Berghe, T. V.; Vandenabeele, P. and Kroemer, G. The molecular machinery of regulated cell death. *Cell Res.* **2019**, *29*,347–364.

Thein, K.H.; Kleylein-Sohn, J.; Nigg, E.A.; Gruneberg, U. Astrin is required for the maintenance of sister chromatid cohesion and centrosome integrity. *J. Cell Biol.* **2007**, *178*, 345–354.

Tsou, M.F.; Wang, W.J.; George, K.A.; Uryu, K.; Stearns, T.; Jallepalli, P.V. Polo kinase and separase regulate the mitotic licensing of centriole duplication in human cells. *Dev. Cell* **2009**, *17*, 344–354.

Uhlmann, F.; Lottspeich, F.; Nasmyth, K. Sister-chromatid separation at anaphase onset is promoted by cleavage of the cohesin subunit Scc1. *Nature* **1999**, *400*, 37–42.

Uhlmann, F.; Wernic, D.; Poupart, M.A.; Koonin, E.V.; Nasmyth, K. Cleavage of cohesin by the CD clan protease separin triggers anaphase in yeast. *Cell* **2000**, *103*, 375–386.

Waizenegger, I.; Giménez-Abián, J.F.; Wernic, D.; Peters, J.-M. Regulation of human separase by securin binding and autocleavage. *Curr. Biol.* **2002**, *12*, 1368–1378.

Wolf, F.; Wandke, C.; Isenberg, N. and Geley, S. Dose-dependent effects of stable cyclin B1 on progression through mitosis in human cells. *EMBO J.* **2006**, *25*, 2802–2813.

Yu, J.; Raia, P.; Ghent, C.M.; Raisch, T.; Sadian, Y.; Cavadini, S.; Sabale, P.M.; Barford, D.; Raunser, S.; Morgan, D.O.; et al. Structural basis of human separase regulation by securin and CDK1-cyclin B1. *Nature* **2021**, *596*, 138–142.

Zachariae, W.; Shin, T.H.; Galova, M.; Obermaier, B.; Nasmyth, K. Identification of subunits of the anaphase-promoting complex of *Saccharomyces cerevisiae*. *Sci.* **1996**, *274*, 1201–1204.

Zhang, Z.; Yang, H.; Wu, G.; Li, Z.; Song, T.; Li, XQ. Probing the difference between BH3 groove of Mcl-1 and Bcl-2 protein: implications for dual inhibitors design. *Eur J Med Chem* **2011**, *46*, 3909–16.

Zhang, J.; Wang, X.; Cui, W. Visualization of caspase-3-like activity in cells using a genetically encoded fluorescent biosensor activated by protein cleavage. *Nat. Commun.* **2013**, *4*, 2157.

Zhang, W.; Suzuki, M.; Ito, Y.; Douglas, K.T. A Chemically Modified Green-Fluorescent Protein that Responds to Cleavage of an Engineered Disulphide Bond by Fluorescence Resonance Energy Transfer (FRET)-Based Changes. *Chem. Lett.* **2005**, *34*, 766–767.

Zhang, P.; Zhang, X.; Liu, X.; Khan, S.; Zhou, D.; Zheng, G. PROTACs are effective in addressing the platelet toxicity associated with BCL-XL inhibitors. *Explor Target Antitumor Ther.* **2020**, *1*, 259-72.

Zou, H.; Stemman, O.; Anderson, J.S.; Mann, M.; Kirschner, M.W. Anaphase specific auto-cleavage of separase. *FEBS Lett.* **2002**, *528*, 246–250.

Appendix 1

Amino acid sequence

Amino acid sequences for molecular sensor of separase including NLS marked with red for NLS, yellow for adjusted linker, blue for separase recognition sequence, green for dye attached cysteine. In case of WNLS, GFP with simply removed GPKKKRKV. In case of amino acid sequences for GFP and RFP based molecular sensor of caspase-3, recognition sequence of caspase-3, DEVD and original linker sequences were denoted with blue and pink respectively. Amino acid sequences for molecular sensor of caspase-9 is comparably marked with blue for recognition sequence (LEHD) and yellow for referred linker sequences.

MASMTGGQQMGR **GPKKKRKV** MSKGEELFTG VVPILVELDG DVNGHKFSVS
GEGEGDATYG KLTLKFISTT GKLPVPWPTL VTTLTYGVQC FSRYPDHMKR
HDFFKSAMPE GYVQERTISF KDDGNYKTRA EVKFEGDTLV NRIELKGIDF
KEDGNILGHK LEYNYNSHNV YTTADKQKNG IKANFKTRHN IEDGSVQLAD
HYQQNTPIGD GPVLLPDNHY LSTQSALLKD PNEKRDHMVL LEFVTAAG**SGSSG**
DREIMREGTC ELYK GG HHHHHH

MASMTGGQQMGR MSKGEELFTG VVPILVELDG DVNGHKFSVS GEGEGDATYG
KLTLKFISTT GKLPVPWPTL VTTLTYGVQC FSRYPDHMKR HDFFKSAMPE
GYVQERTISF KDDGNYKTRA EVKFEGDTLV NRIELKGIDF KEDGNILGHK
LEYNYNSHNV YTTADKQKNG IKANFKTRHN IEDGSVQLAD HYQQNTPIGD
GPVLLPDNHY LSTQSALLKD PNEKRDHMVL LEFVTAAGSGIT **DEVDGTC** ELYK GG
HHHHHH

MASSEDVIKE FMRFKVRMEG SVNGHEFEIE GEGEGRPYEG TQTAKLKVTK
GGPLPFAWDI LSPQFQYGSK VYVKHPADIP DYKKLSFPEG FKWERVMNFE
DGGVVTVTQD SSLQDGEFIY KVKFIGVNFY SDGPVMQKKT MGWEPSTERL
YPRDGVKKE IHKALKKLDG GHYLVEFKSI YMAKKPVQLP GYYYVDSKLD
ITSHNEDYTI VEQYERTEGR HHLFLSGT **DEVDGTC**CGG HHHHHH

MASMTGGQQMGR MSKGEELFTG VVPILVELDG DVNGHKFSVS GEGEGDATYG
KLTLKFISTT GKLPVPWPTL VTTLTYGVQC FSRYPDHMKR HDFFKSAMPE
GYVQERTISF KDDGNYKTRA EVKFEGDTLV NRIELKGIDF KEDGNILGHK
LEYNYNSHNV YTTADKQKNG IKANFKTRHN IEDGSVQLAD HYQQNTPIGD
GPVLLPDNHY LSTQSALLKD PNEKRDHMVL LEFVTAAG**SGSSGIT** **LEHDGTC** ELYK
GG HHHHHH

Appendix 2

Table 2: Some molecular sensors Förster radius estimated value are shown in Appendix 2

Estimated Förster Radius					
Probe type	J(l) (M-1cm ³)	n ⁴	eA(MAX)	QYD	R ₀ (nm) [k ² = 2/3]
GFP(caspase-3)-Alexa Fluor 532	1.27E-11	0.32	81000	0.68	10.8
GFP(caspase-3)-Alexa Fluor 546	1.03E-11	0.32	104000	0.68	10.5
GFP(caspase-3)-Alexa Fluor 555	2.05E-11	0.32	150000	0.68	11.7
GFP(caspase-3)-Alexa Fluor 594	5.63E-12	0.32	73000	0.68	9.5
GFP(caspase-3)-Alexa Fluor 633	6.45E-12	0.32	239000	0.68	9.7
GFP(caspase-3)-Alexa Fluor 647	7.83E-12	0.32	132000	0.68	10.0
GFP(caspase-3)-Alexa Fluor 660	3.65E-12	0.32	184000	0.68	8.8
GFP(caspase-3)-Alexa Fluor 750	9.89E-13	0.32	240000	0.68	7.1

Appendix 3. Identification of different cell states upon NLS based molecular sensor uptake by fluorescence microscopic observation in detail

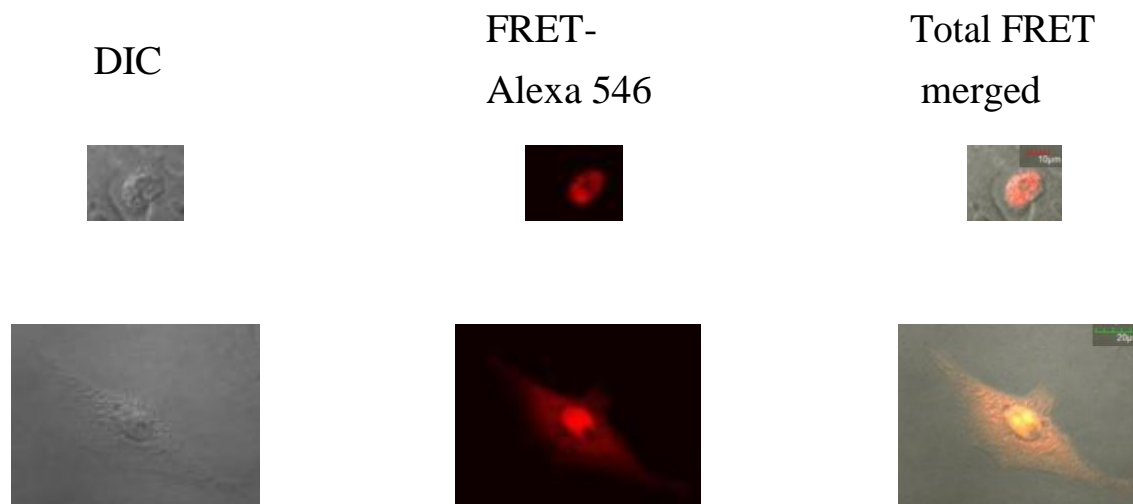


Figure 14: Identification of different cell states upon NLS based molecular sensor uptake using fluorescence microscopic observations in detail. Although forms of introduced cells were varied as a spherical shape or spread one, they still exhibited identical localization patterns for molecular sensors.